NASA TECHNICAL NOTE

NASA TN D-4084

NASA TN D-4084

FREE-STREAM INTERFERENCE EFFECTS ON EFFECTIVENESS OF CONTROL JETS NEAR THE WING TIP OF A VTOL AIRCRAFT MODEL

by Kenneth P. Spreemann

Langley Research Center

Langley Station, Hampton, Va.

NATIONAL AERONAUTICS AND SPACE ADMINISTRATION • WASHINGTON, D. C. • AUGUST 1967

NASA TN D-4084

FREE-STREAM INTERFERENCE EFFECTS ON EFFECTIVENESS OF CONTROL JETS NEAR THE WING TIP OF A VTOL AIRCRAFT MODEL

By Kenneth P. Spreemann

Langley Research Center
Langley Station, Hampton, Va.

NATIONAL AERONAUTICS AND SPACE ADMINISTRATION

For sale by the Clearinghouse for Federal Scientific and Technical Information
Springfield, Virginia 22151 – CFSTI price $3.00

FREE-STREAM INTERFERENCE EFFECTS ON EFFECTIVENESS OF CONTROL JETS NEAR THE WING TIP OF A VTOL AIRCRAFT MODEL

By Kenneth P. Spreemann
Langley Research Center

SUMMARY

An investigation in the transition speed range of the free-stream interference effects on control jets at the wing tip and at an inboard location of a model of a jet VTOL aircraft has been conducted in the 7- by 10-foot test section of the Langley 300-MPH 7- by 10-foot tunnel. The results showed that interference effects of the jets and free stream induced losses in the effective roll control; however, these losses were reduced as the jets were moved rearward and toward the wing tip. Sideslipping the wing forward or upstream gave negative (unfavorable) interference increments in rolling moment, whereas sideslipping the wing backward or downstream gave positive (favorable) increments. Aileron deflection had very little effect on the interference effects between the jets and free stream.

INTRODUCTION

Much research has been done in the development of VTOL aircraft for use in areas where conventional take-off and landing cannot be accomplished. Jet aircraft are of great interest when mission requirements demand high subsonic or supersonic capabilities. It is apparent that in the low transition speed range, conventional controls are inadequate because of the low dynamic pressures passing over the control surfaces; therefore, artificial controls of some nature must be incorporated in the aircraft under consideration. Thus, for jet aircraft, small jets supplied by bleed off from the main engine or engines located at the nose and tail for pitch and yaw and at the wing tips for roll are usually used as a means of providing the required control in this speed range.

For roll control, these jets would logically be placed beneath the wing tips. Because of their small size relative to the wing area, a significant loss in control effectiveness, resulting from adverse interference effects, would be expected. It has been documented in a number of investigations, such as references 1 to 5, that jets issuing normal from flat or approximately flat surfaces cause losses in lift and nose-up pitching moments at

forward speed because of the induced pressures on the surface surrounding the jet and that these lift losses and pitching moments increase with increasing surface area. The basic causes of these phenomena are fully discussed in the references and thus are not discussed further in this paper.

The present investigation is confined to jet and free-stream interference effects that would affect roll control of jet VTOL aircraft in the transition speed range. This investigation was conducted on a wing-fuselage combination with various arrangements of nozzles emitting beneath the right wing at the tip and at an inboard location. The tests were made in the 7- by 10-foot section of the Langley 300-MPH 7- by 10-foot tunnel from very low to moderate forward speeds.

SYMBOLS

The force and moment data are presented about the stability axes. The positive sense of forces, moments, and angles is indicated in figure 1. Moments of the model are referred to the assumed centers of gravity indicated by figure 2. The units of measure used in this paper are given both in the U.S. Customary System and, parethetically, in the International System (SI). Details concerning the use of SI, together with physical constants and conversion factors, are given in reference 6.

b	wing span, ft (m)
c	local wing chord, ft (m)
$\bar{c}$	wing mean aerodynamic chord, $\frac{2}{S}\int_0^{b/2} c^2 dy$, ft (m)
C_p	pressure coefficient, $\frac{p - p_\infty}{q_\infty}$
ΔC_p	increment in pressure coefficient, $(C_p)_{\text{jet on}} - (C_p)_{\text{jet off}}$
M_X	moment about X-axis, ft-lbf (m-N)
ΔM_X	increment in moment about X-axis, $(M_X)_{\text{jet on}} - (M_X)_{\text{jet off}}$, ft-lbf (m-N)
p	pressure, lbf/ft^2 (N/m^2)
q	dynamic pressure, lbf/ft^2 (N/m^2)
r	radius of the fuselage at x distance from the nose, in. (m)

S	wing area, ft^2 (m^2)
T	thrust, lbf (N)
V	velocity, ft/sec (m/sec)
x	distance along the X-axis from the nose, in. (m)
y	spanwise distance from plane of model symmetry, ft (m)
α	model angle of attack with respect to fuselage reference line, deg
β	angle of sideslip, deg
δ	control deflection, deg
ρ	mass density of air, slugs/ft^3 (kg/m^3)

Subscripts:

a	aileron
j	jet
o	wind off
∞	free stream

MODEL AND APPARATUS

Drawings of the two model configurations showing the general arrangements with pertinent dimensions are given in figure 2. Photographs of the short-span configuration are presented in figure 3. The right wing only was provided with a plenum chamber and a system of nozzles, pressure orifices, and an aileron. The nozzles were designed with an exit angle for an optimum Mach number of 1.4. The pressure orifices were located on the wing lower surface just inboard of the nozzles. Detailed arrangements of the nozzles, plenum chamber, pressure orifices, and aileron are given in figure 4. The model was mounted on a six-component strain-gage balance for measurements of the forces and moments.

The wings, which were mounted in the fuselage in the midposition, had aspect ratios of 2.89 and 3.56, taper ratios of 0.419 and 0.329, leading-edge sweep of 45°, and NACA 65-210 airfoil sections parallel to the plane of symmetry. Details of the fuselage are given in table I. The aspect-ratio-2.89 wing was constructed so that a longer span configuration could be made by removing the rounded wing tips and attaching an extended outboard section, and thus simulating an inboard system of nozzles. The right wing only had a 20-percent-chord aileron.

TESTS

The sting-supported model was tested in the 7- by 10-foot test section of the Langley 300-MPH 7- by 10-foot tunnel at free-stream velocities of 50 ft/sec (15.24 m/sec) to 360 ft/sec (109.7 m/sec). The Reynolds numbers based on the wing mean aerodynamic chord and tunnel velocity varied from 0.58×10^6 to 4.25×10^6. The investigation covered sideslip angles of 0° to $\pm 30^{\circ}$. For all test conditions the model was held constant at an angle of attack of 0°.

On a typical run the nozzle pressure ratio was held constant while the tunnel speed was varied to cover the transition speed range. The nozzles were usually operated in consecutive pairs to provide high thrust for greater accuracy in the data. The average measured static thrust T_o for a pair of nozzles was 18 pounds (80.0064 N) for $\frac{p_j}{p_\infty} = 3.6$ and 36 pounds (160.128 N) for $\frac{p_j}{p_\infty} = 6.0$. The thrust at the higher pressure ratio varied ±1 percent around the mean value whereas at the lower pressure the variation was ±2 percent.

PRESENTATION OF RESULTS

The results of the investigation are presented in the following figures:

The pressure distributions in figures 14 to 19 were selected at two lower effective velocity ratios for figures 5 to 7, 9, and 10 as an indication of the type of pressure field

encountered in the critical transition speed range. Since the coverage of the wing surface was very limited, these pressures are intended to provide only a qualitative picture of the flow field around the jets. More detailed coverage and discussions of the pressure distribution on a flat plate surrounding a jet are given in references 3 and 4.

RESULTS AND DISCUSSION

As previously mentioned, only the rolling moments and a few typical pressure distributions near the jets are considered in this paper. The rolling moments presented in this investigation were nondimensionalized by the measured rolling moment at zero tunnel velocity. For the two thrust levels investigated, the tunnel speed was varied through a range to give effective velocity ratios $\sqrt{\frac{\rho_\infty V_\infty^2}{\rho_j V_j^2}}$ covering the transition speed range. This effective velocity ratio suggested in reference 7 appears to be an appropriate parameter for comparing cold and hot jets.

Effects of Jet Position and Presssure Ratio

Shown in figures 5 and 7 are the effects of jet positions for pressure ratios of 3.6 and 6.0 for the jets at the wing tip and a pressure ratio of 6.0 for the jets inboard of the wing tip. As the jets are moved rearward on the wing chord, the adverse interference effects are reduced at zero sideslip. Figure 6 gives the effects of the jets at the wing tip, and figure 7 shows the effects of inboard location of the jets. The additional area beyond the jets just about doubled the interference effects at 0° sideslip in the high transition speed range but showed little change due to sideslip.

Moving the jets rearward and to the wing tip reduces the critical area behind and beside the jets and hence alleviates the adverse interference effects. (See figs. 5 to 7.) Thus, it is apparent that the jets should be located as near the wing tip and trailing edge as possible. The static pressures on the wing lower surface adjacent to the jets, plotted in figures 14 to 16, clearly show the large negative pressure field moving aft with the movement of the jets.

Comparing figure 5 $\left(\frac{p_j}{p_\infty} = 3.6\right)$ with figure 6 $\left(\frac{p_j}{p_\infty} = 6.0\right)$, shows that at 0° and -30° sideslip the interference losses affecting the rolling moment were essentially unaffected by pressure ratio; however, at 30° sideslip, the interference losses were somewhat greater at the higher pressure ratio.

Effects of Sideslip

Only one wing was instrumented and provided with control jets. When sideslip conditions were investigated, positive sideslip was used to simulate the conditions

encountered by the jets on the forward or upstream wing and negative sideslip was used to simulate the conditions on the downstream or trailing wing.

The data for 0° and $\pm 30^{\circ}$ of sideslip are compared in figures 8 to 10 which show much larger adverse interference effects (losses in control effectiveness) for positive sideslip. However, favorable interference effects (an increase in control effectiveness) are shown for negative sideslip. Some effects of sideslip are to be expected inasmuch as the area behind the jet is increased for positive sideslip and decreased for negative sideslip. This simple analysis, however, does not explain the large favorable effects at negative sideslip. The pressure-distribution data (figs. 18 and 19) show a reduction in suction pressure at negative sideslip but no positive pressures, which are apparently present elsewhere on the wing to produce the favorable interference effects. (See also ref. 8.)

The reduction in control effectiveness occurs in the 60- to 100-knot speed range where the interference between the primary lift jets and the free stream causes a large increase in effective dihedral (increase in rolling moment with speed, ref. 9) and the need for control is increased. This reduced control effectiveness is alleviated by the effects of sideslip because the control required to trim out the rolling moment due to sideslip requires use of the control jets on the trailing or downstream wing (which corresponds to the negative sideslip case in the present investigation) on which favorable interference effects are experienced for downward-directed control jets. The effectiveness of an upward-directed jet on the forward or upstream wing would be greatly reduced by the interference effects (similar to that shown by the data for positive sideslip).

Effects of Aileron Deflection

The total or basic rolling moment (which includes jet, aileron, and interference) is presented in figure 11, and the rolling-moment data due to aileron deflection only are presented in figure 12. The data in figure 12 are for the power-off condition but are nondimensionalized based on the power-on condition to facilitate direct comparison with the rest of the data. The interference on rolling moment due to deflecting the aileron was obtained from the following expression:

$$\frac{\Delta M_{X_{\delta_a}}}{T_o y} = \left[\left(M_{X_{\delta_a}}\right)_{\text{jet on}}\right] - \left[\left(M_{X_{\delta_a}}\right)_{\text{jet off}} + \left(M_{X_{\delta_a=0}}\right)_{\text{jet on}}\right]$$

in which the first term is the data of figure 11, the second term is from figure 12, and the third term is the data of figure 6(a) for the respective nozzle positions. The resulting interference $\Delta M_{X_{\delta_a}}/T_o y$ presented in figure 13 clearly shows that there was no mutual interference between the aileron and control jet except at the most negative aileron deflection and higher effective velocity ratios where some small effects can be noted.

CONCLUSIONS

An investigation made in the transition speed range to determine some of the interference effects between jets for roll control located beneath the wing at the tip and inboard of the tip and free stream for a VTOL model indicated the following conclusions:

1. Mutual interference effects of the jets and free stream induced losses in the effective roll control; however, these losses were reduced as the jets were moved rearward on the wing chord and to the wing tip.

2. Sideslipping the wing forward or upstream gave negative (unfavorable) interference increments in rolling moment, whereas sideslipping the wing backward or downstream gave positive (favorable) increments.

3. Aileron deflection had very little effect on the mutual interference effects between the jets and the free stream.

Langley Research Center,
National Aeronautics and Space Administration,
Langley Station, Hampton, Va., February 2, 1967,
721-01-00-18-23.

REFERENCES

1. Spreemann, Kenneth P.: Induced Interference Effects on Jet and Buried-Fan VTOL Configurations in Transition. NASA TN D-731, 1961.

2. Spreemann, Kenneth P.: Investigation of Interference of a Deflected Jet With Free Stream and Ground on Aerodynamic Characteristics of a Semispan Delta-Wing VTOL Model. NASA TN D-915, 1961.

3. Bradbury, L. J. S.; and Wood, M. N.: The Static Pressure Distribution Around a Circular Jet Exhausting Normally From a Plane Wall into an Airstream. C.P. No. 822, Brit. A.R.C., 1965.

4. Vogler, Raymond D.: Surface Pressure Distributions Induced on a Flat Plate by a Cold Air Jet Issuing Perpendicularly From the Plate and Normal to a Low-Speed Free-Stream Flow. NASA TN D-1629, 1963.

5. Vogler, Raymond D.: Interference Effects of Single and Multiple Round or Slotted Jets on a VTOL Model in Transition. NASA TN D-2380, 1964.

6. Mechtly, E. A.: The International System of Units – Physical Constants and Conversion Factors. NASA SP-7012, 1964.

7. Williams, John; and Butler, Sidney F. J.: Further Developments in Low-Speed Wind-Tunnel Techniques for VSTOL and High-Lift Model Testing. AIAA Aerodynamic Testing Conf., Mar. 1964, pp. 17-32.

8. Kuhn, Richard E.; and McKinney, Marion O., Jr.: NASA Research on the Aerodynamics of Jet VTOL Engine Installations. Aerodynamics of Power Plant Installation, Pt. II, AGARDograph 103, Oct. 1965, pp. 689-713.

9. Margason, Richard J.: Jet-Induced Effects in Transition Flight. Conference on V/STOL and STOL Aircraft, NASA SP-116, 1966, pp. 177-189.

TABLE I.- DETAILS OF FUSELAGE

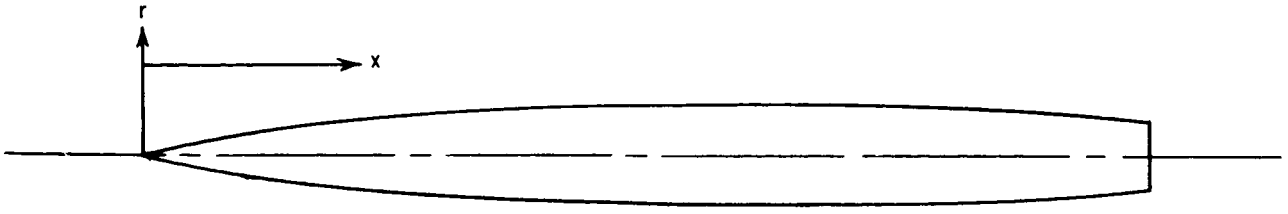

Fuselage coordinates			
Inches		Meters	
x	r	x	r
0	0	0	0
.61	.28	.0155	.0071
.91	.36	.0231	.0091
1.52	.52	.0386	.0132
3.05	.88	.0775	.0224
6.10	1.47	.1549	.0373
9.15	1.97	.2324	.0500
12.20	2.40	.3099	.0610
18.29	3.16	.4646	.0803
24.39	3.77	.6195	.0958
30.49	4.23	.7744	.1074
36.59	4.56	.9294	.1158
42.68	4.80	1.0840	.1219
48.78	4.95	1.2390	.1257
54.88	5.05	1.3940	.1283
60.98	5.08	1.5489	.1290
67.07	5.04	1.7026	.1280
73.17	4.91	1.8585	.1247
79.27	4.69	2.0135	.1191
85.37	4.34	2.1684	.1102
91.46	3.81	2.3231	.0968
100.00	3.35	2.5400	.0851
Nose radius = 0.06 in. (0.00152 m)			

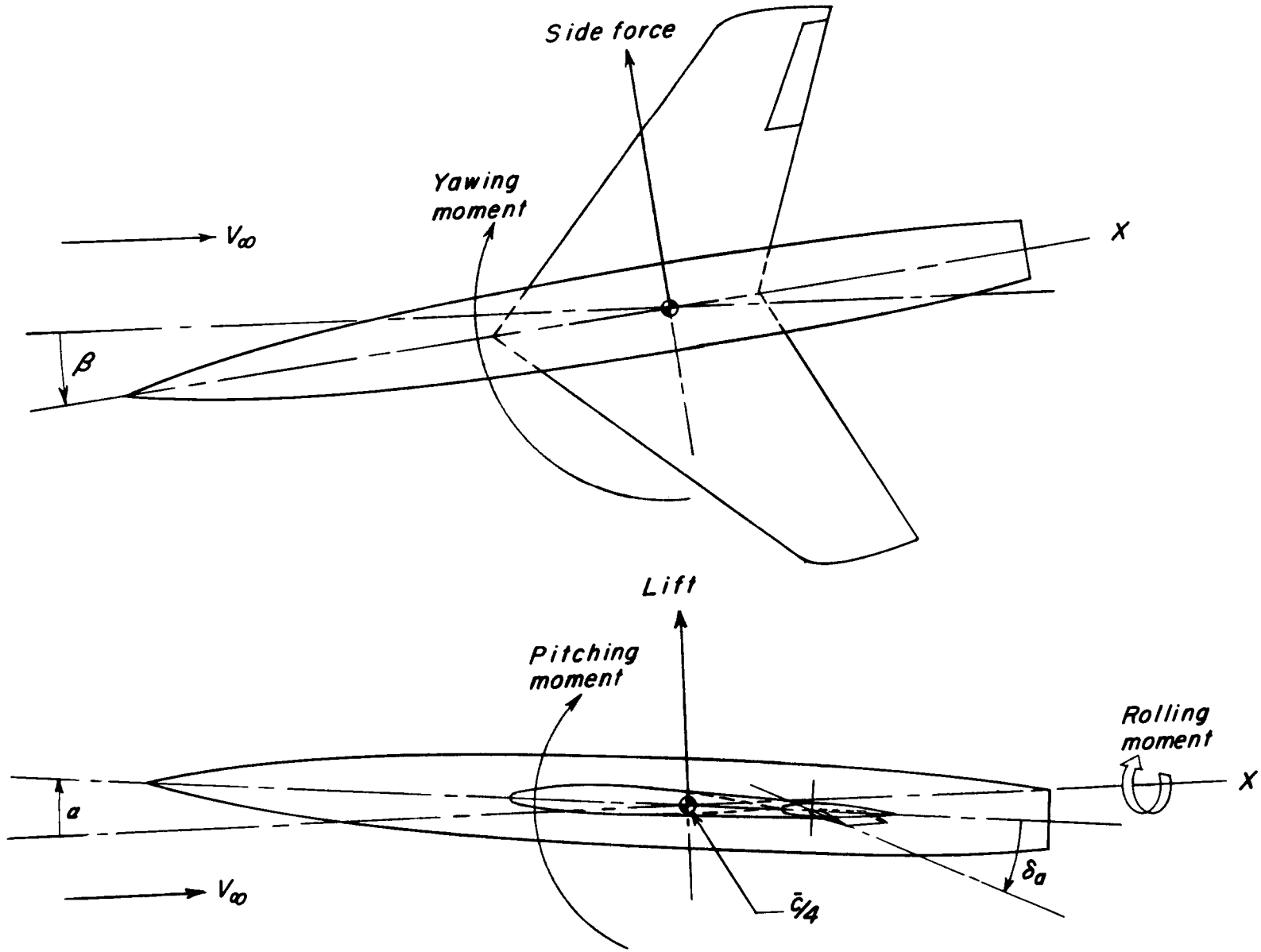

Figure 1.- Reference axes showing positive directions of forces, moments, and angular deflections.

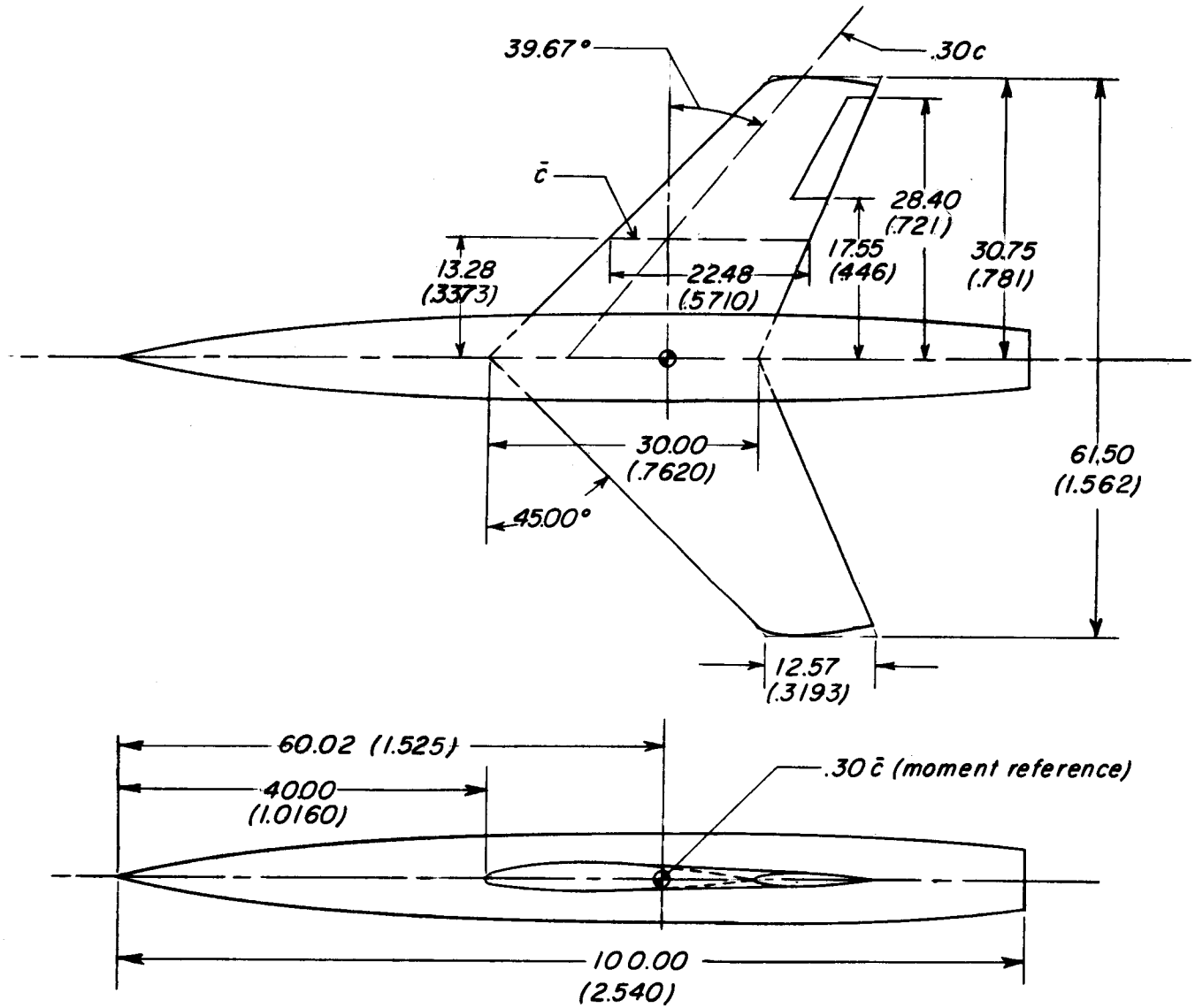

(a) Short-span configuration.

Figure 2.- General arrangement of model configurations investigated. Dimensions are given first in inches and parenthetically in meters.

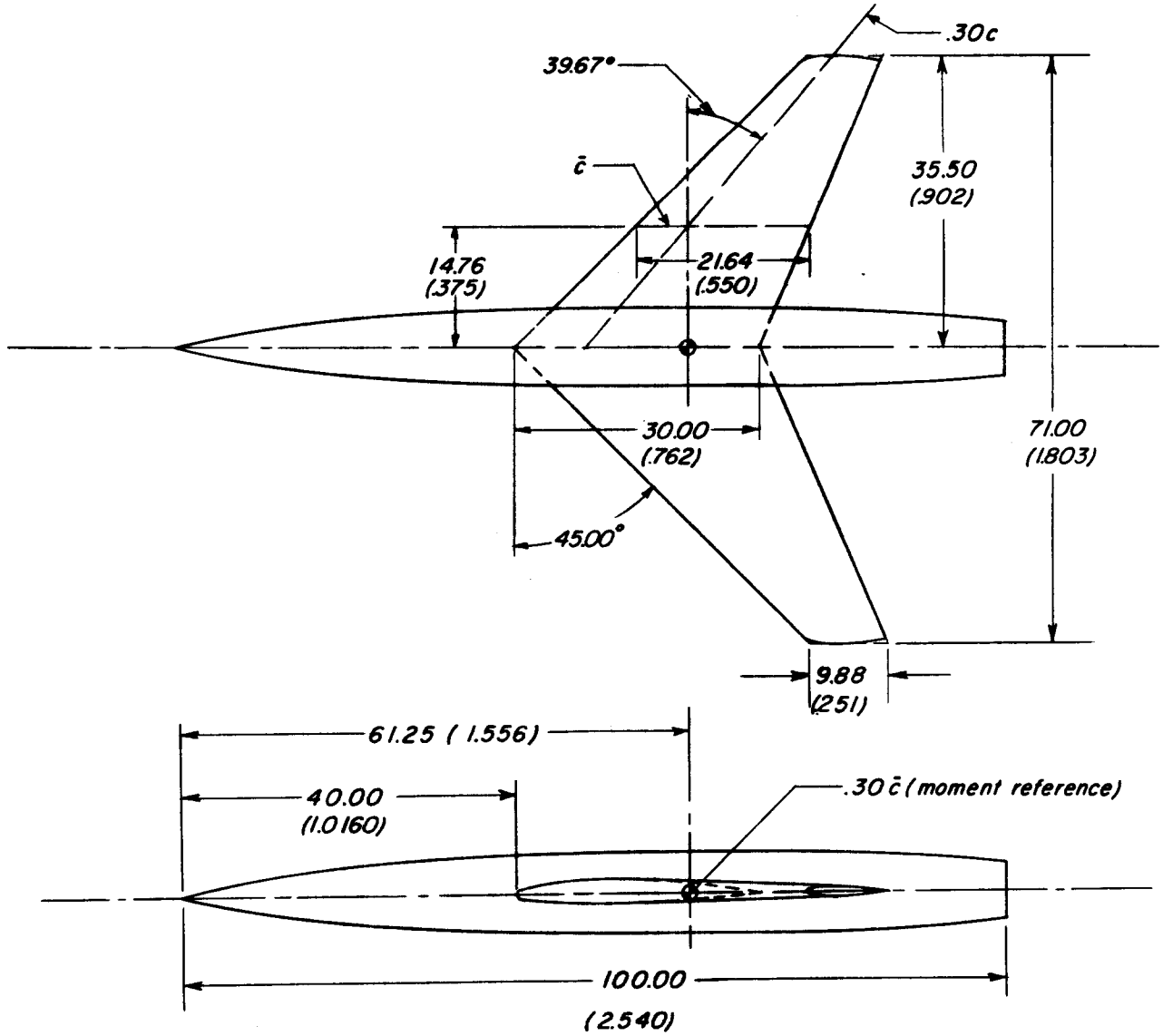

(b) Long (or extended) span configuration.

Figure 2.- Concluded.

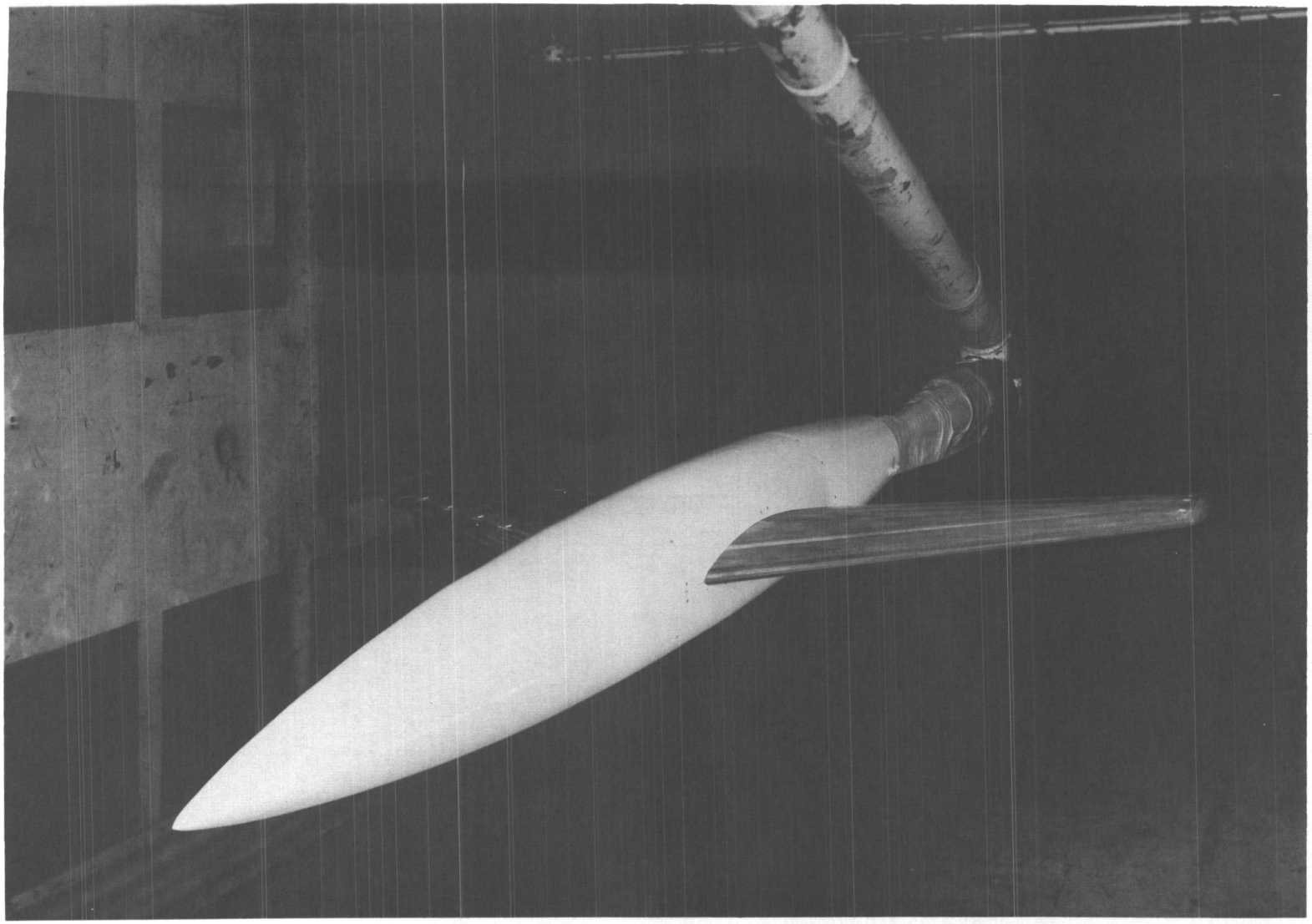

(a) Three-quarter front view. L-65-2783

Figure 3.- Photograph of short-span configuration mounted on sting.

(b) View showing nozzles 1 and 2. L-65-2781

Figure 3.- Continued.

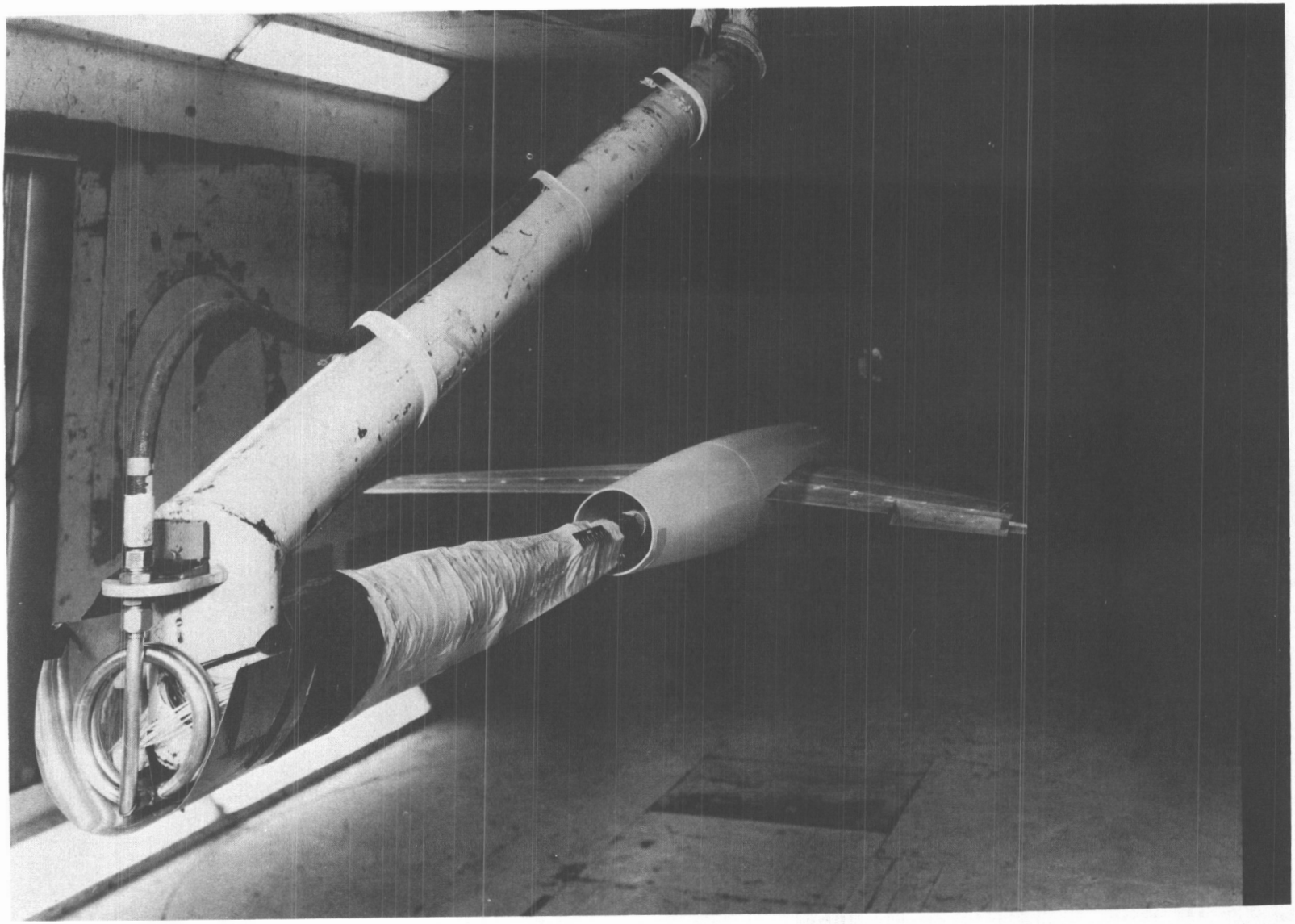

(c) View showing air supply line to model. L-65-2786

Figure 3.- Concluded.

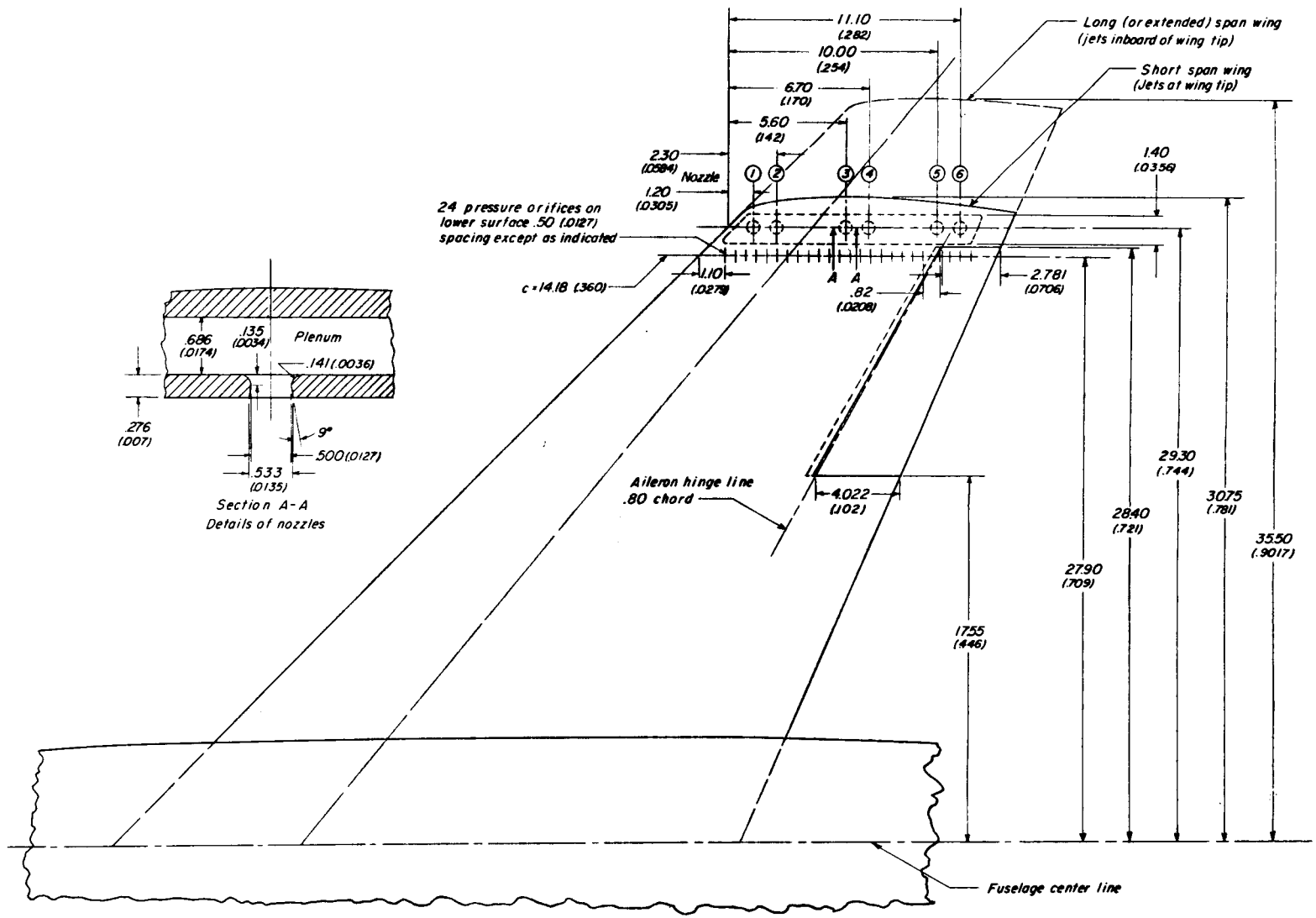

Figure 4.- Sketch of right wing showing arrangements and locations of nozzles and pressure orifices on lower surface. Dimensions are given first in inches and parenthetically in meters.

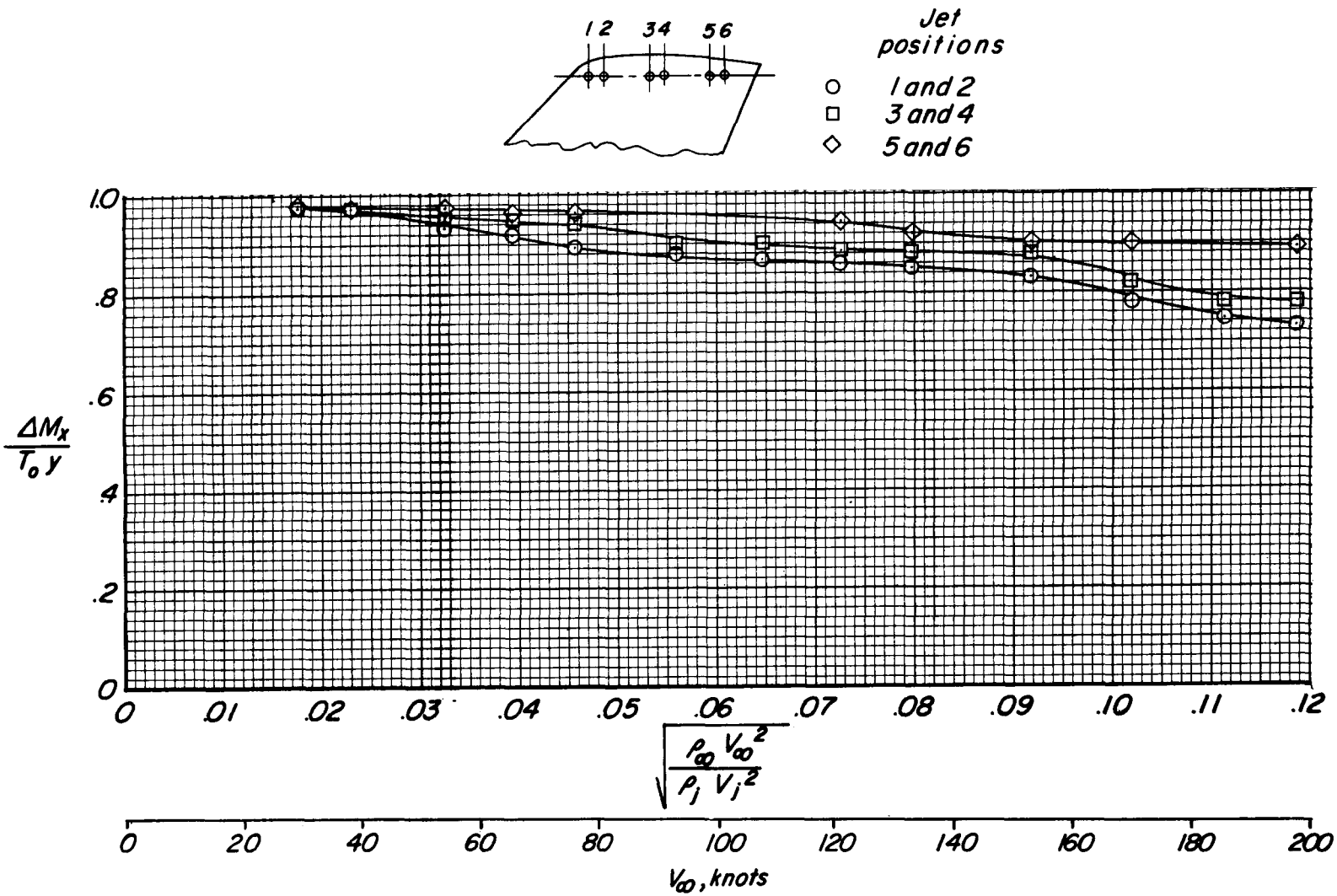

(a) $\beta = 0^0$.

Figure 5.- Effect of jet position on roll control through the transition speed range. Jets at wing tip; $\delta_a = 0^0$; $p_j/p_\infty = 3.6$.

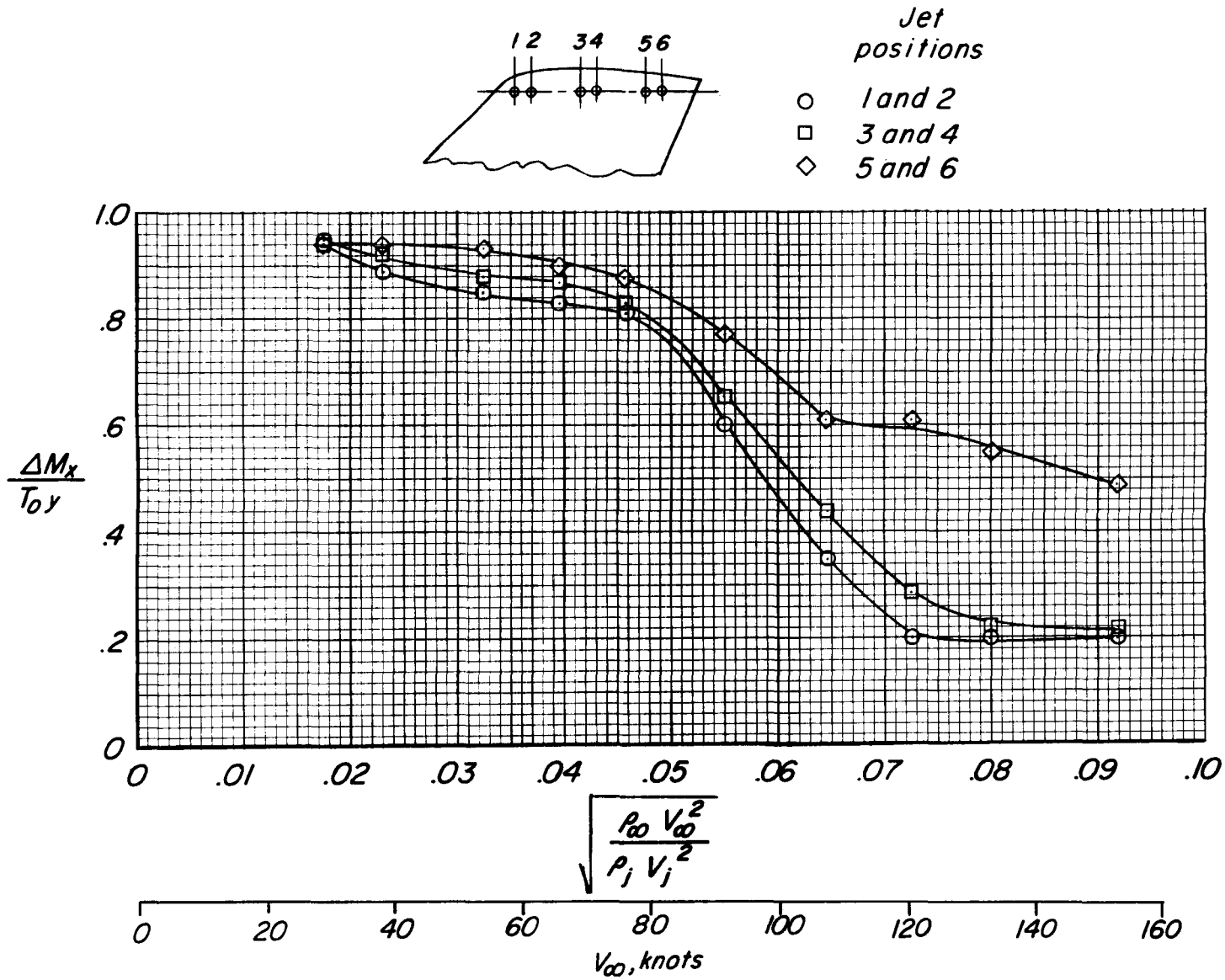

(b) $\beta = 30^0$.

Figure 5.- Continued.

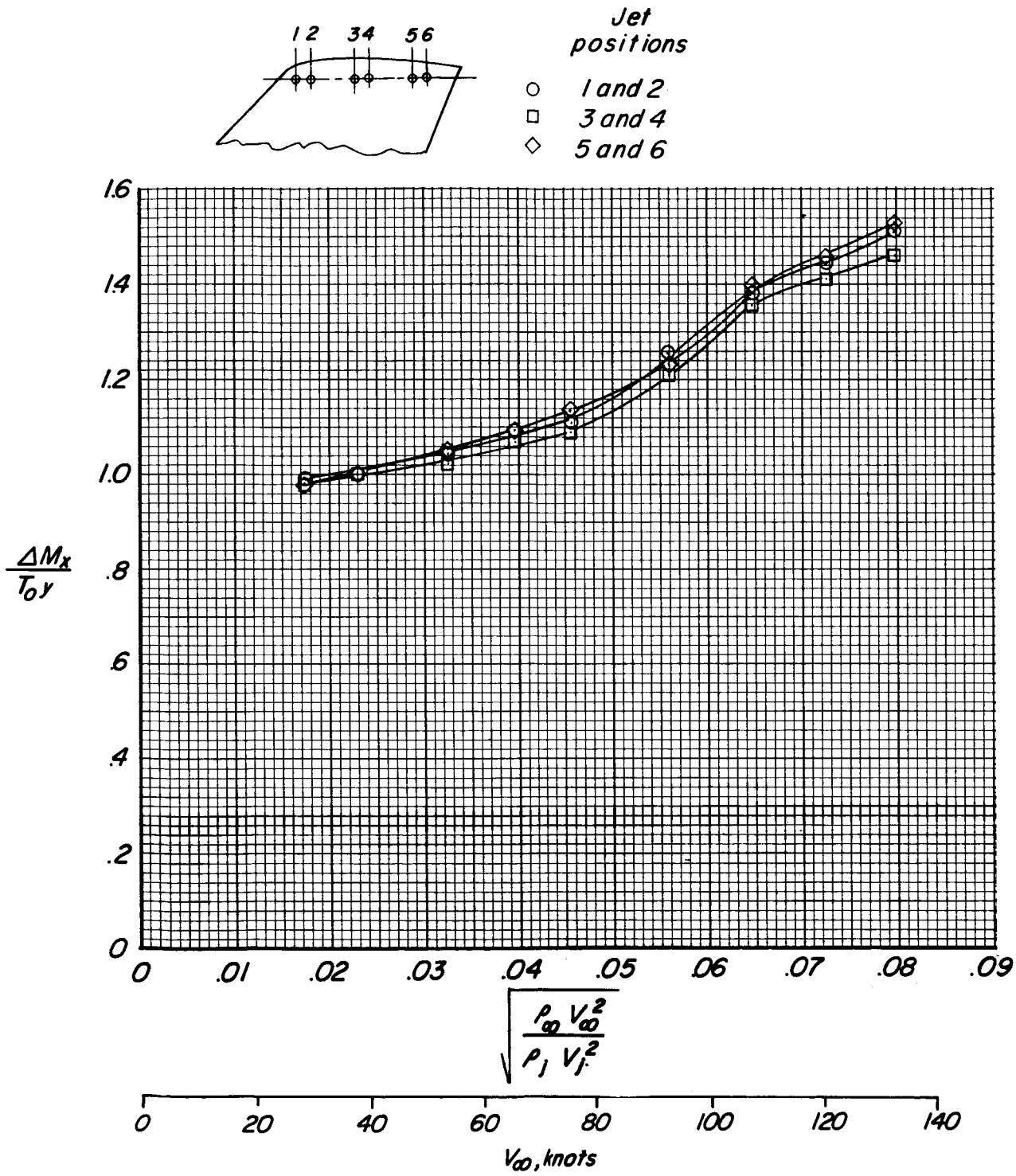

(c) $\beta = -30^0$.

Figure 5.- Concluded.

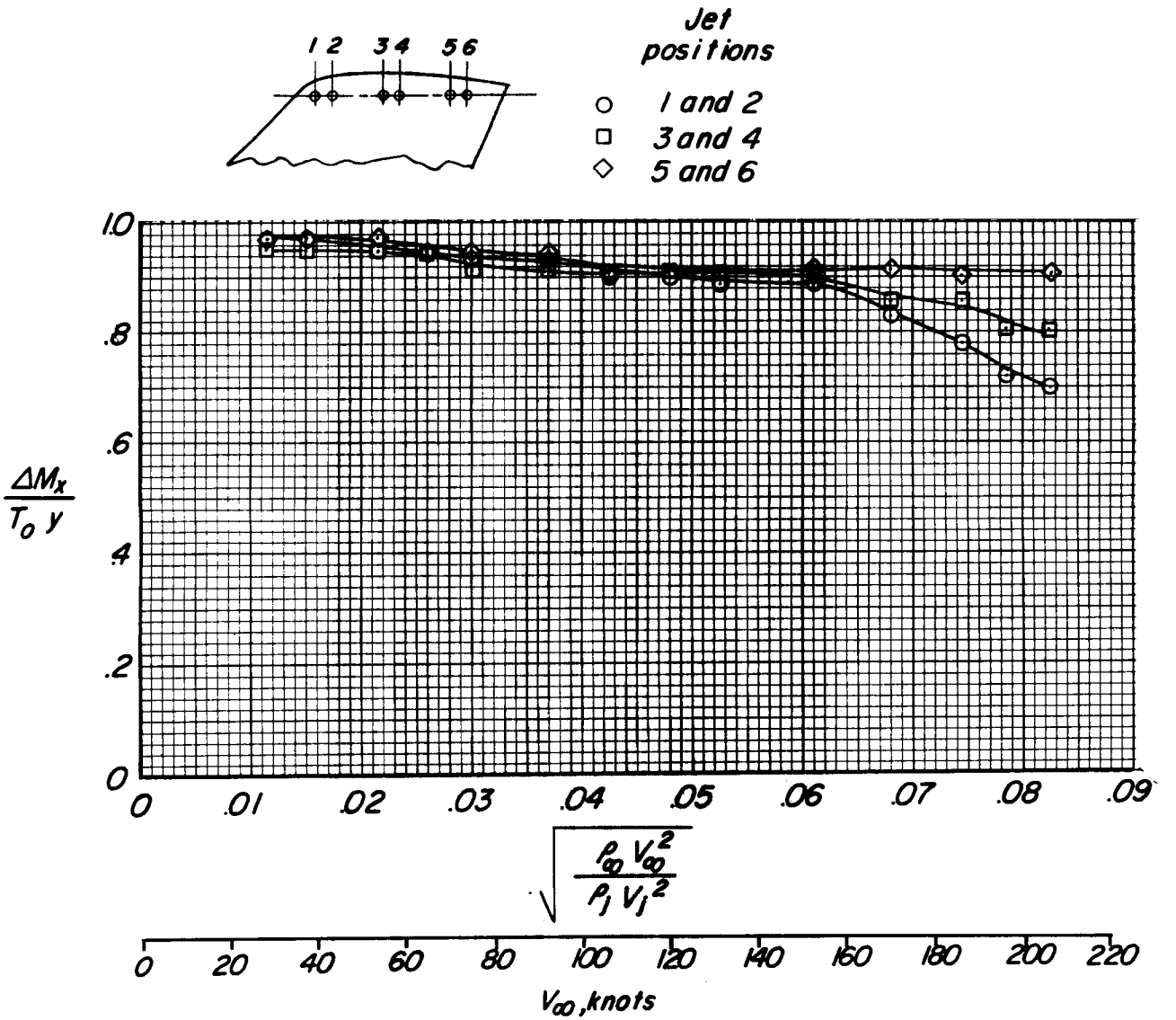

(a) $\beta = 0^{0}$.

Figure 6.- Effect of jet position on roll control through the transition speed range. Jets at wing tip; $\delta_a = 0^{0}$; $p_j/p_\infty = 6.0$.

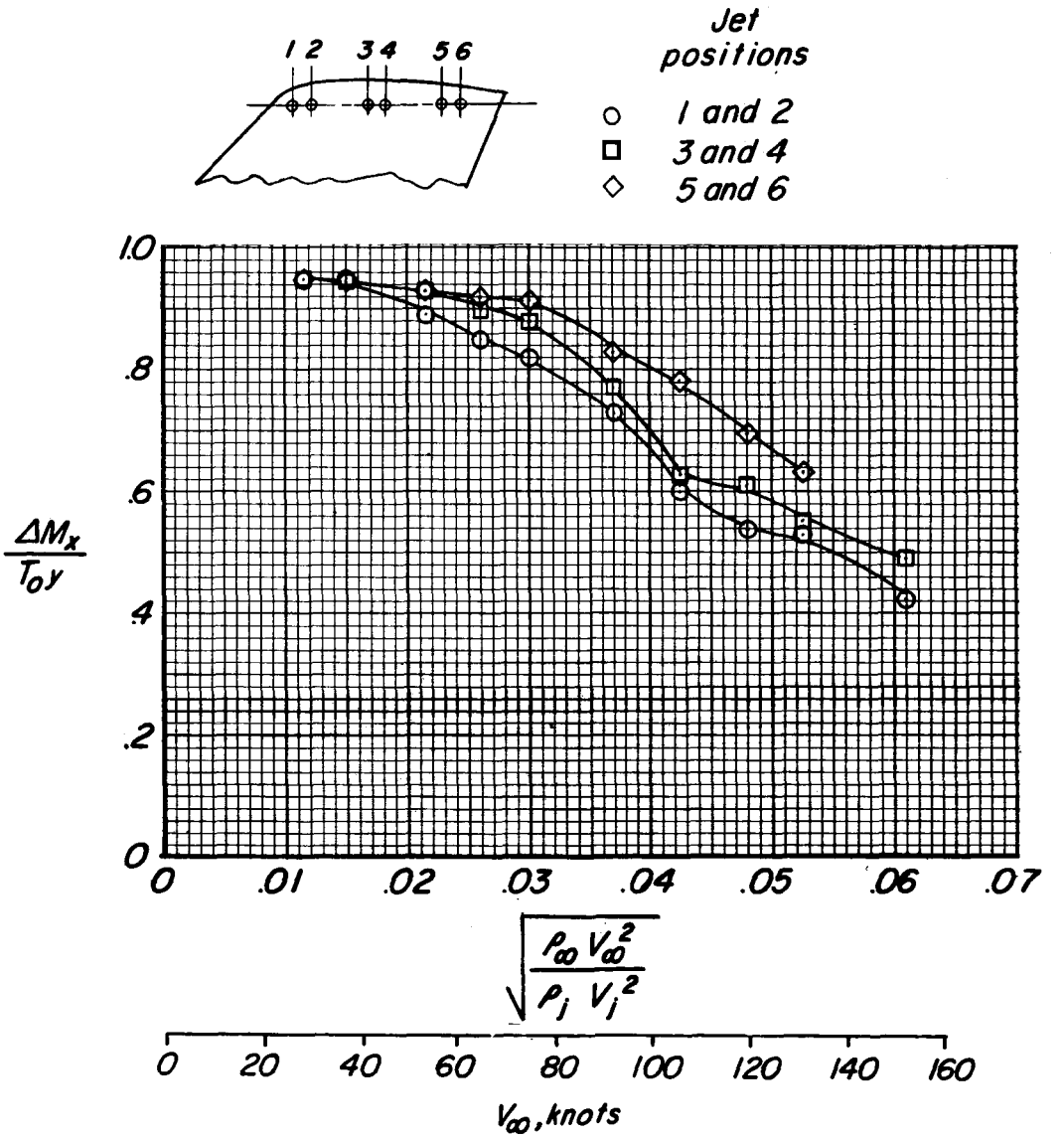

(b) $\beta = 30^0$.

Figure 6.- Continued.

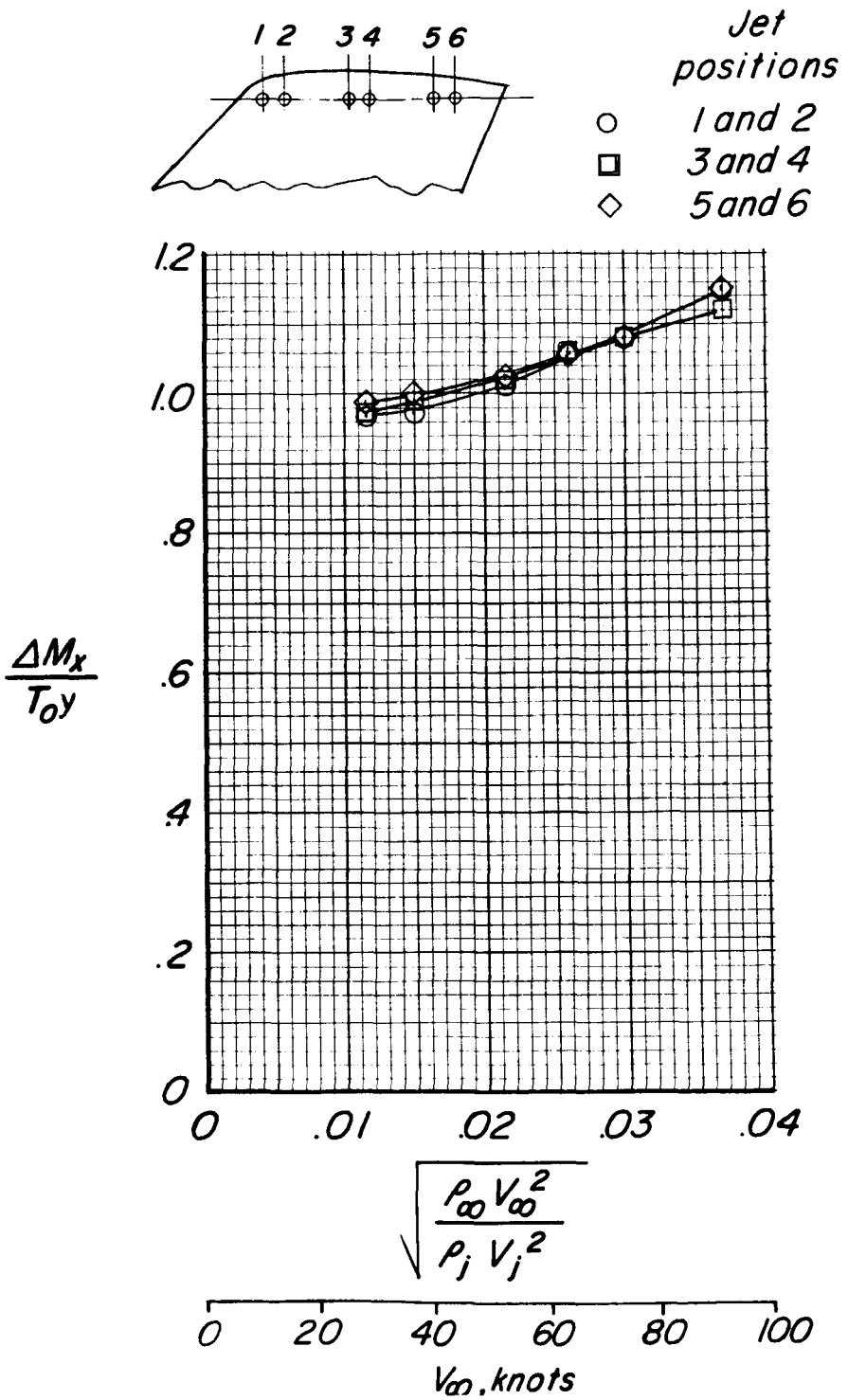

(c) $\beta = -30^{\circ}$.

Figure 6.- Concluded.

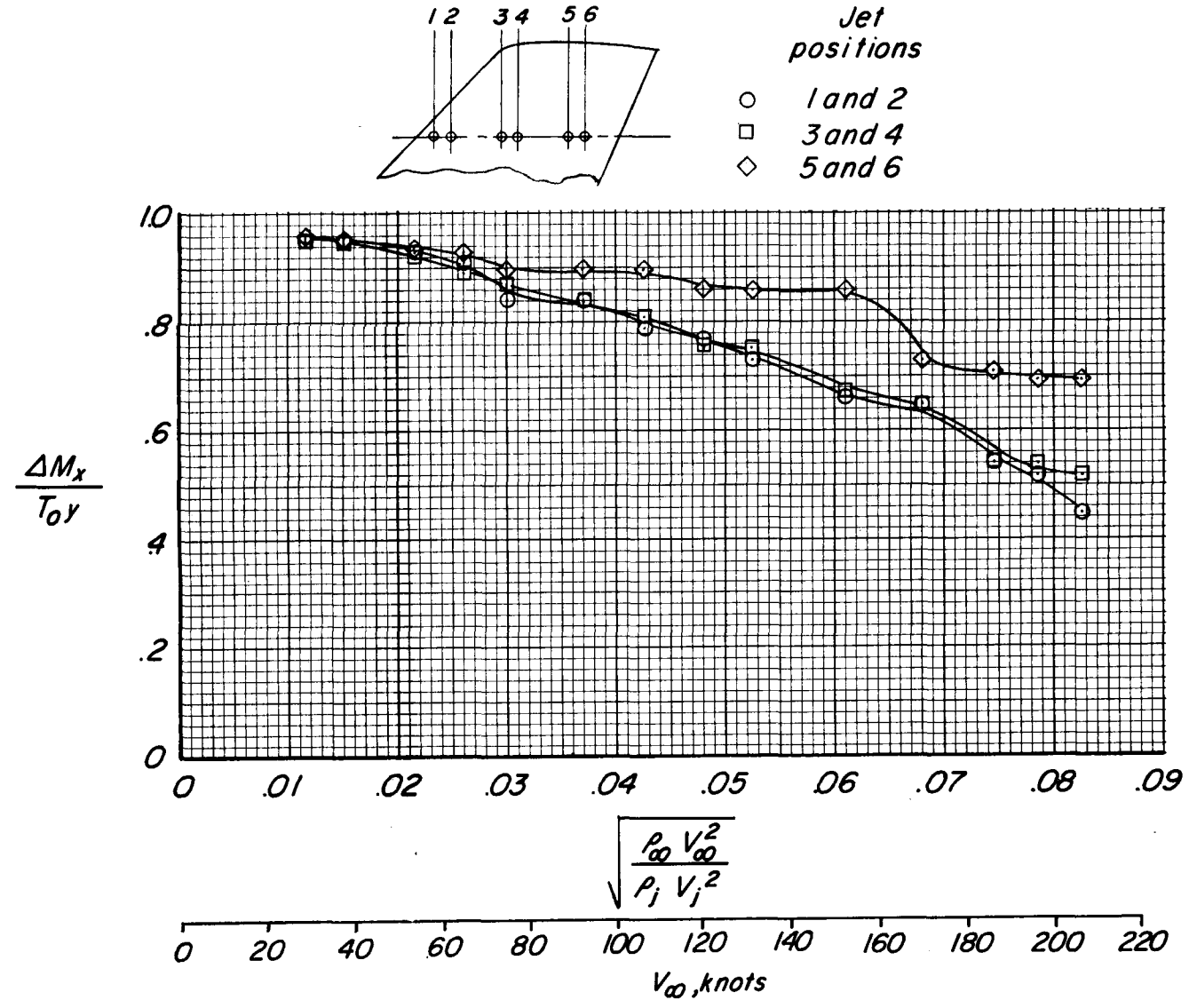

(a) $\beta = 0^0$.

Figure 7.- Effect of jet position on roll control through the transition speed range. Jets inboard of wing tip; $\delta_a = 0^0$; $p_j/p_\infty = 6.0$.

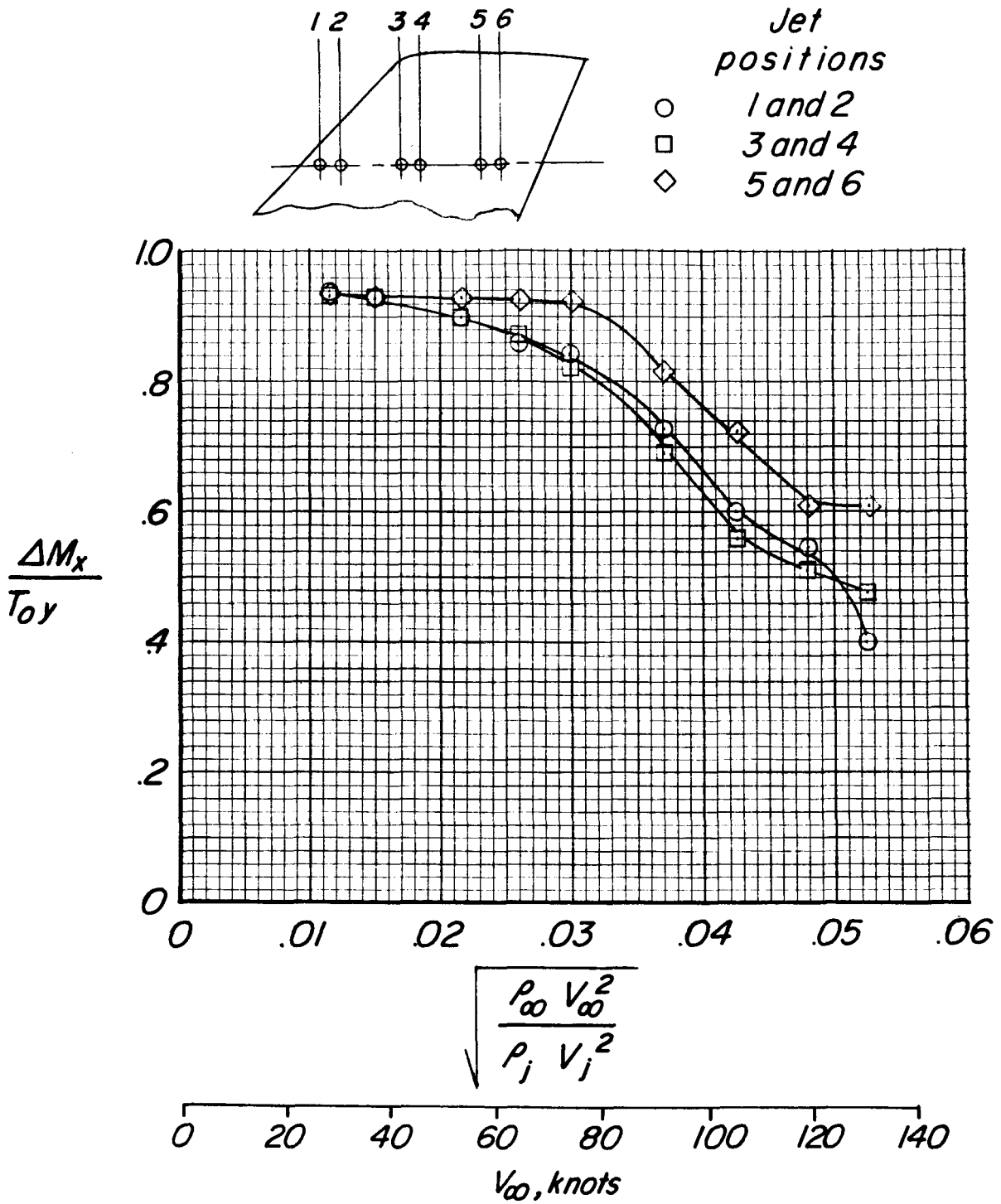

(b) $\beta = 30^{0}$.

Figure 7.- Continued.

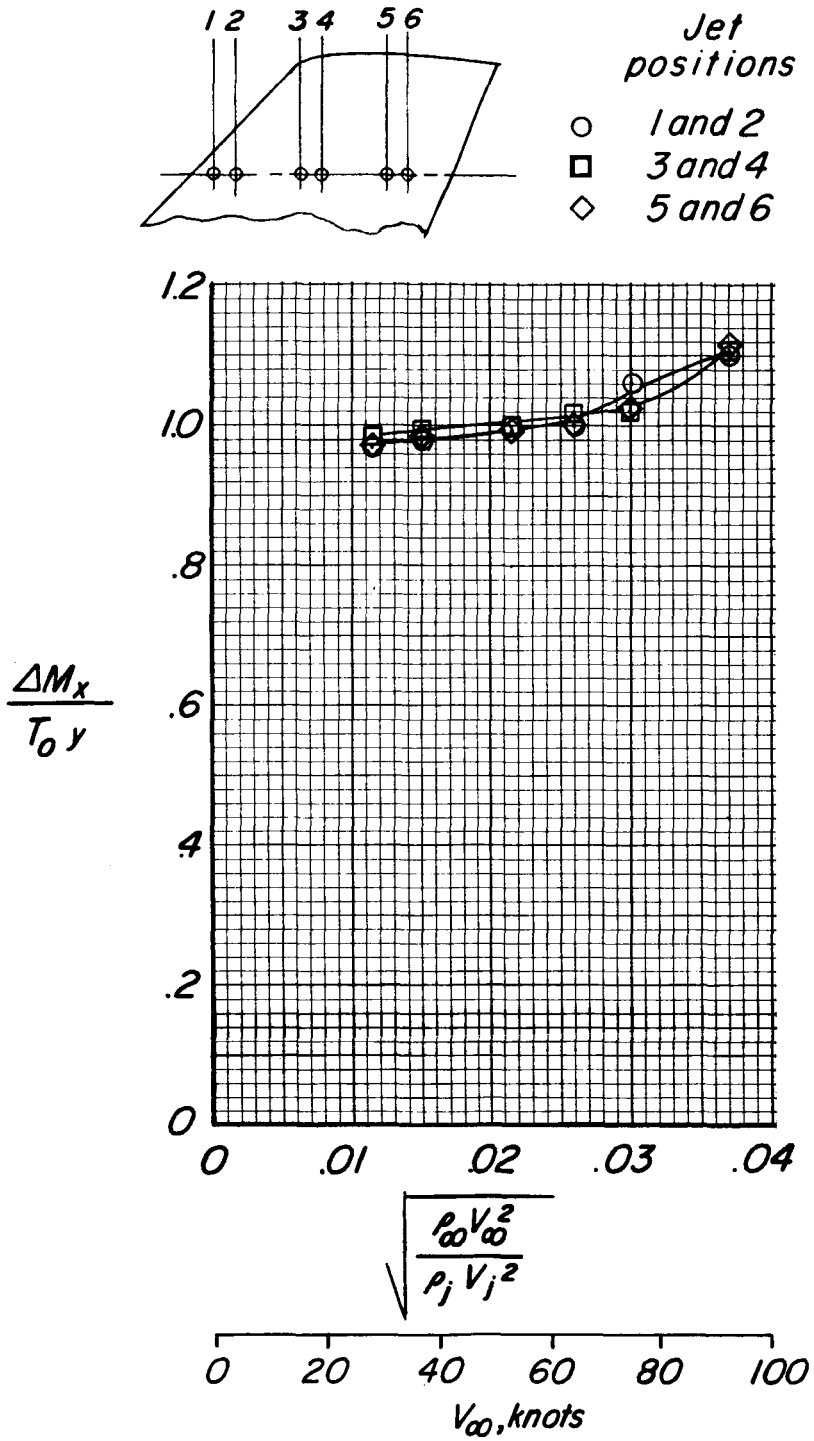

(c) $\beta = -30^0$.

Figure 7.- Concluded.

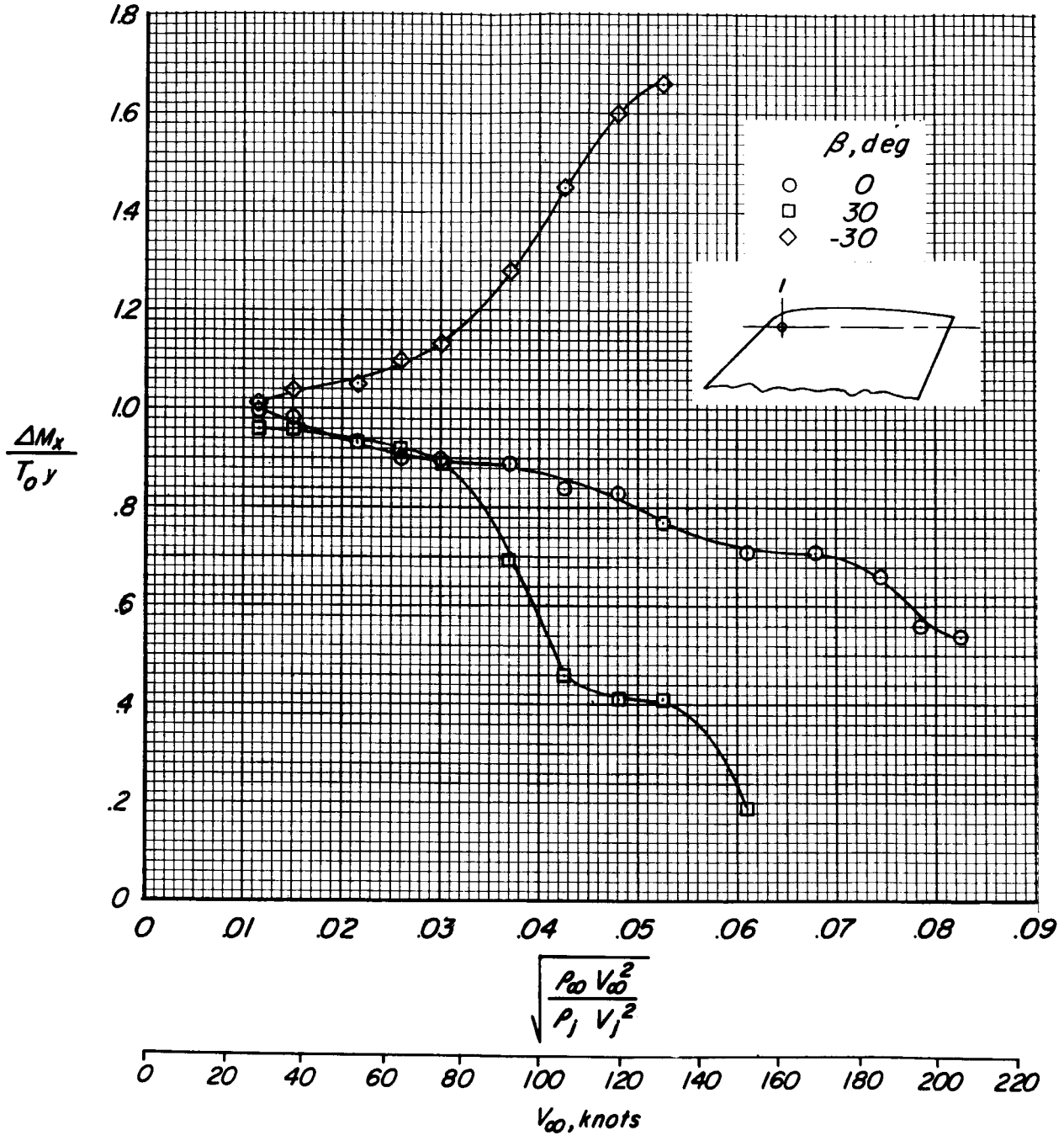

(a) Jet position 1.

Figure 8.- Effect of sideslip on roll control through the transition speed range. Jet at wing tip; $\delta_a = 0^0$; $p_j/p_\infty = 6.0$.

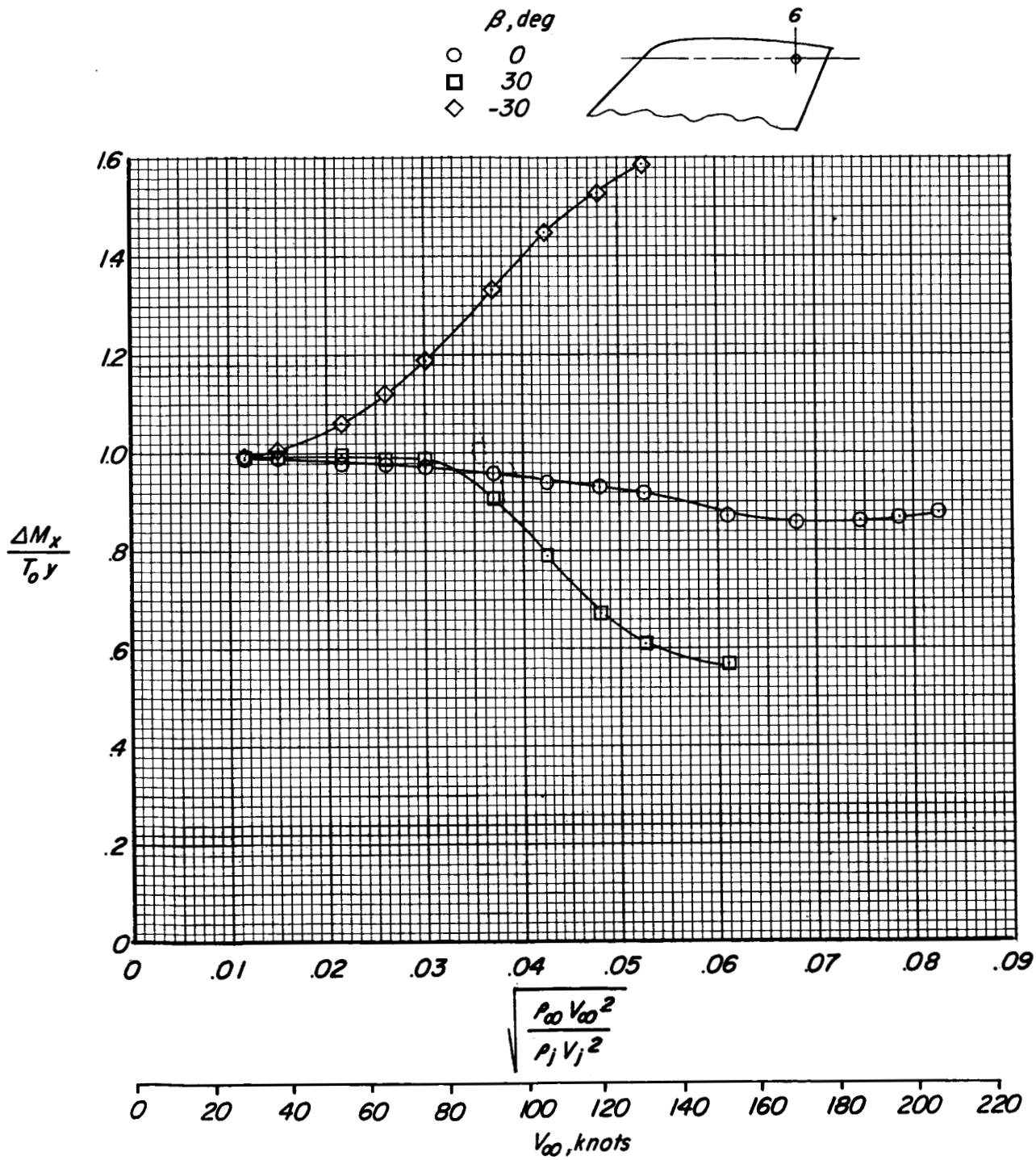

(b) Jet position 6.

Figure 8.- Concluded.

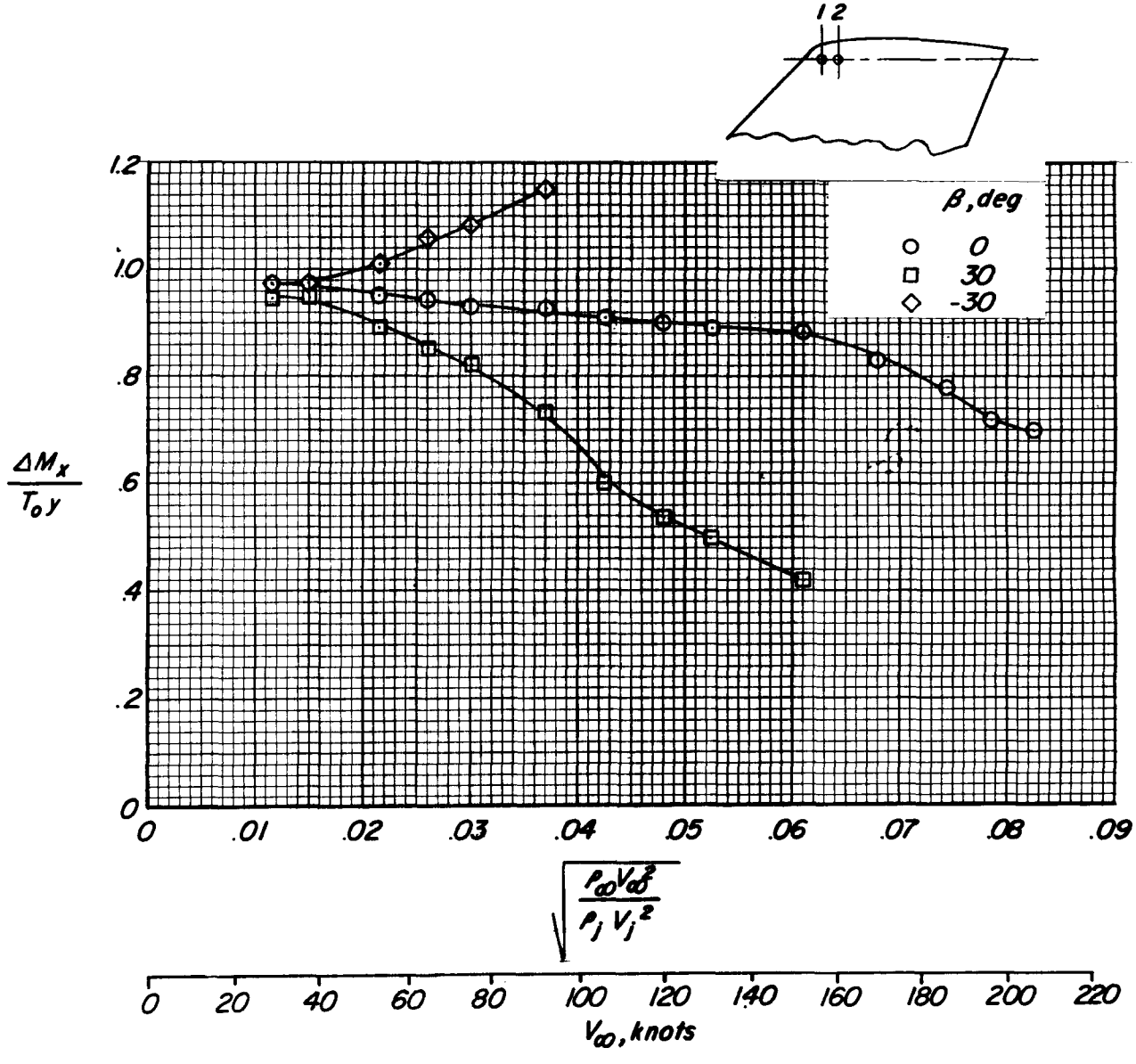

(a) Jet positions 1 and 2.

Figure 9.- Effect of sideslip on roll control through the transition speed range. Jets at wing tip; $\delta_a = 0^0$; $p_j/p_\infty = 6.0$.

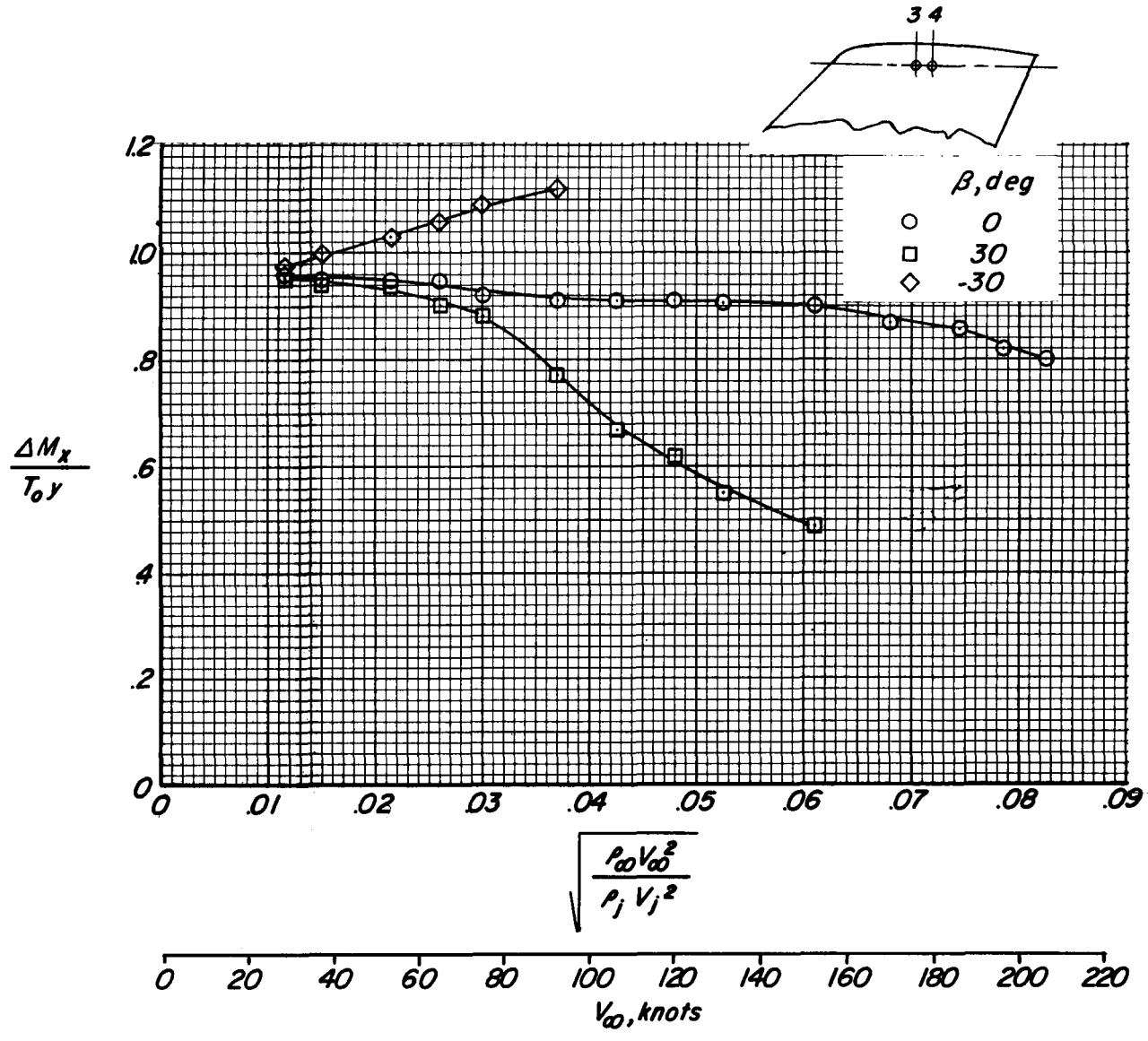

(b) Jet positions 3 and 4.

Figure 9.- Continued.

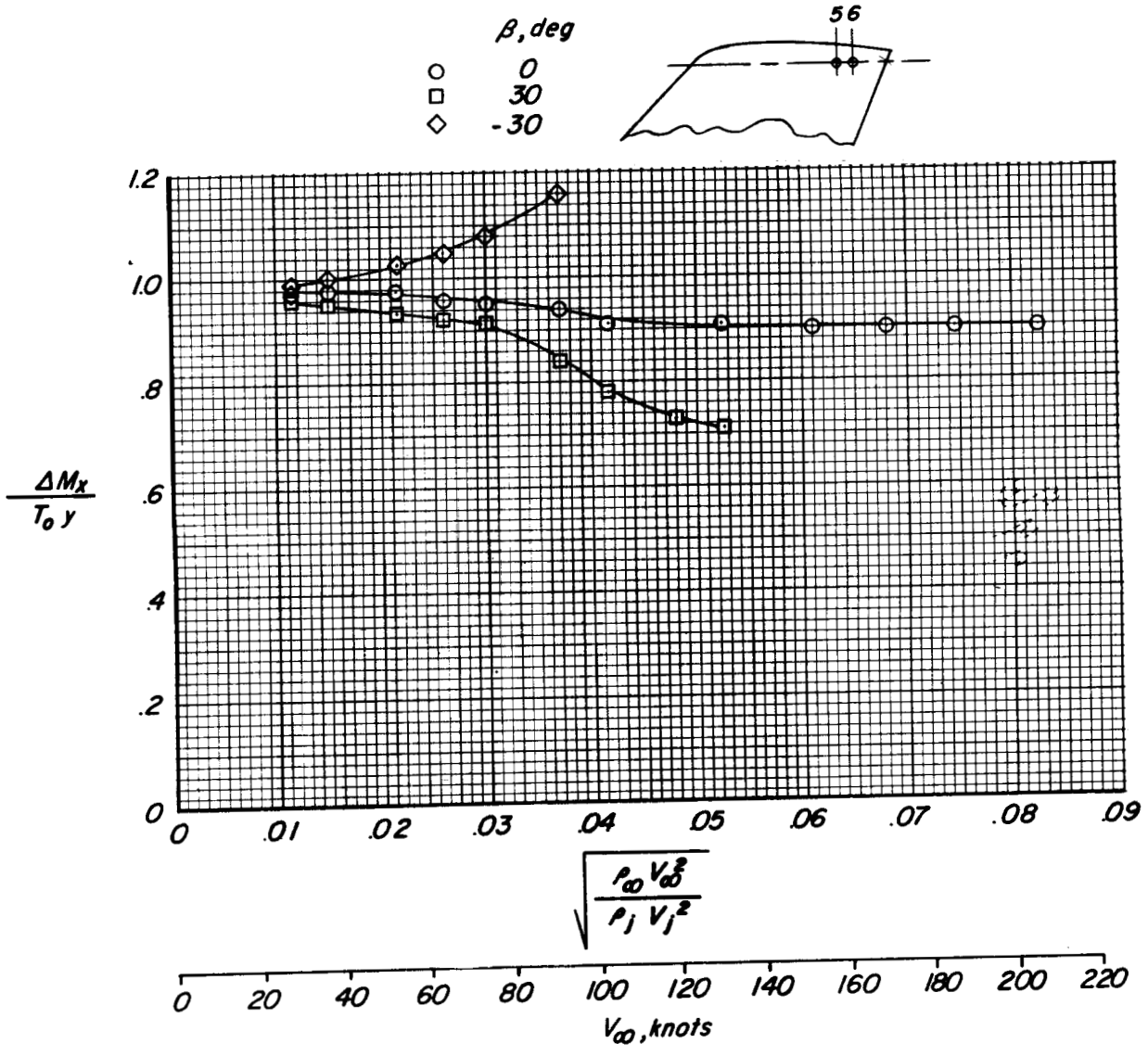

(c) Jet positions 5 and 6.

Figure 9.- Concluded.

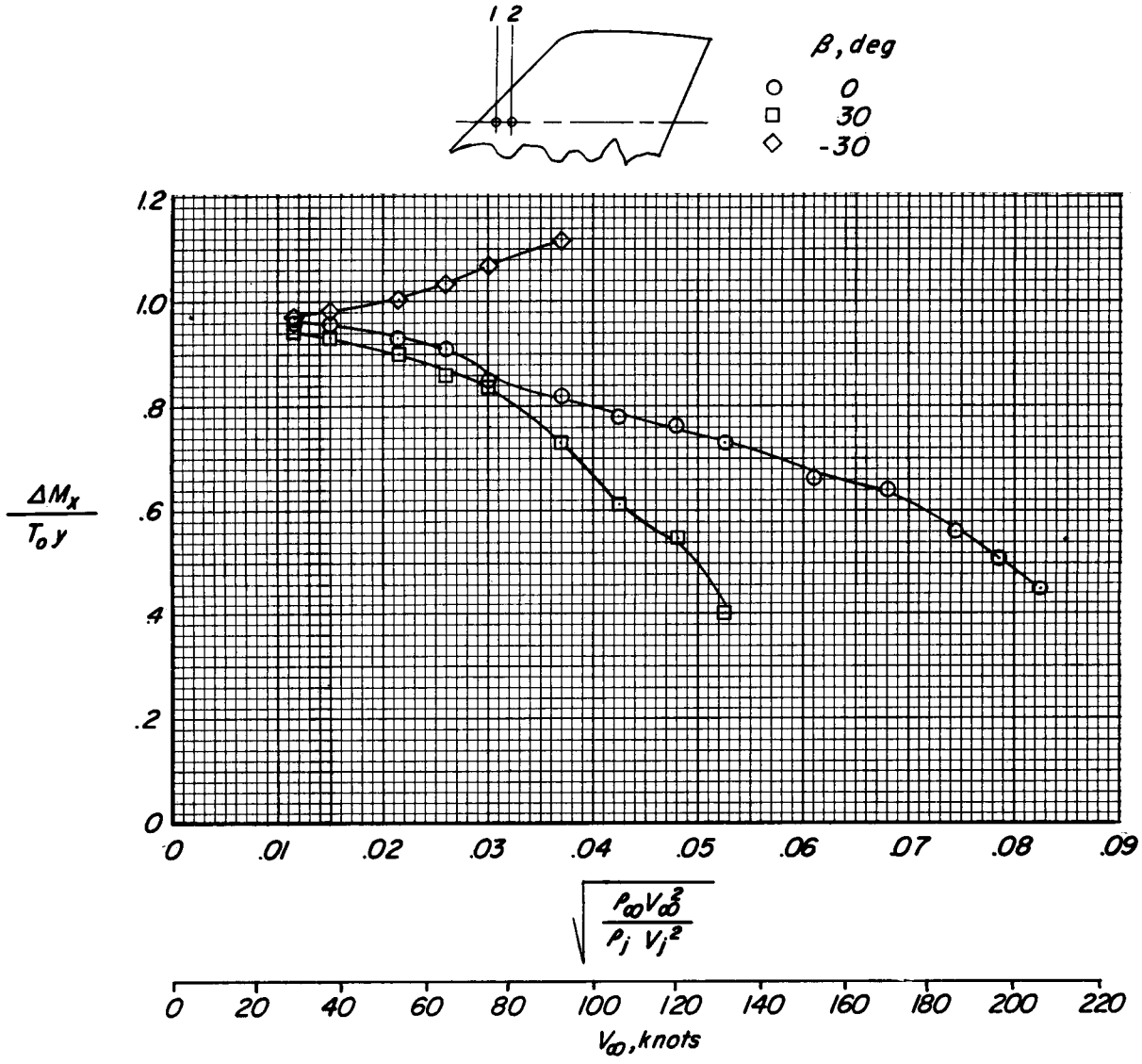

(a) Jet positions 1 and 2.

Figure 10.- Effect of sideslip on roll control through the transition speed range. Jets inboard of wing tip; $\delta_a = 0^0$; $p_j/p_\infty = 6.0$.

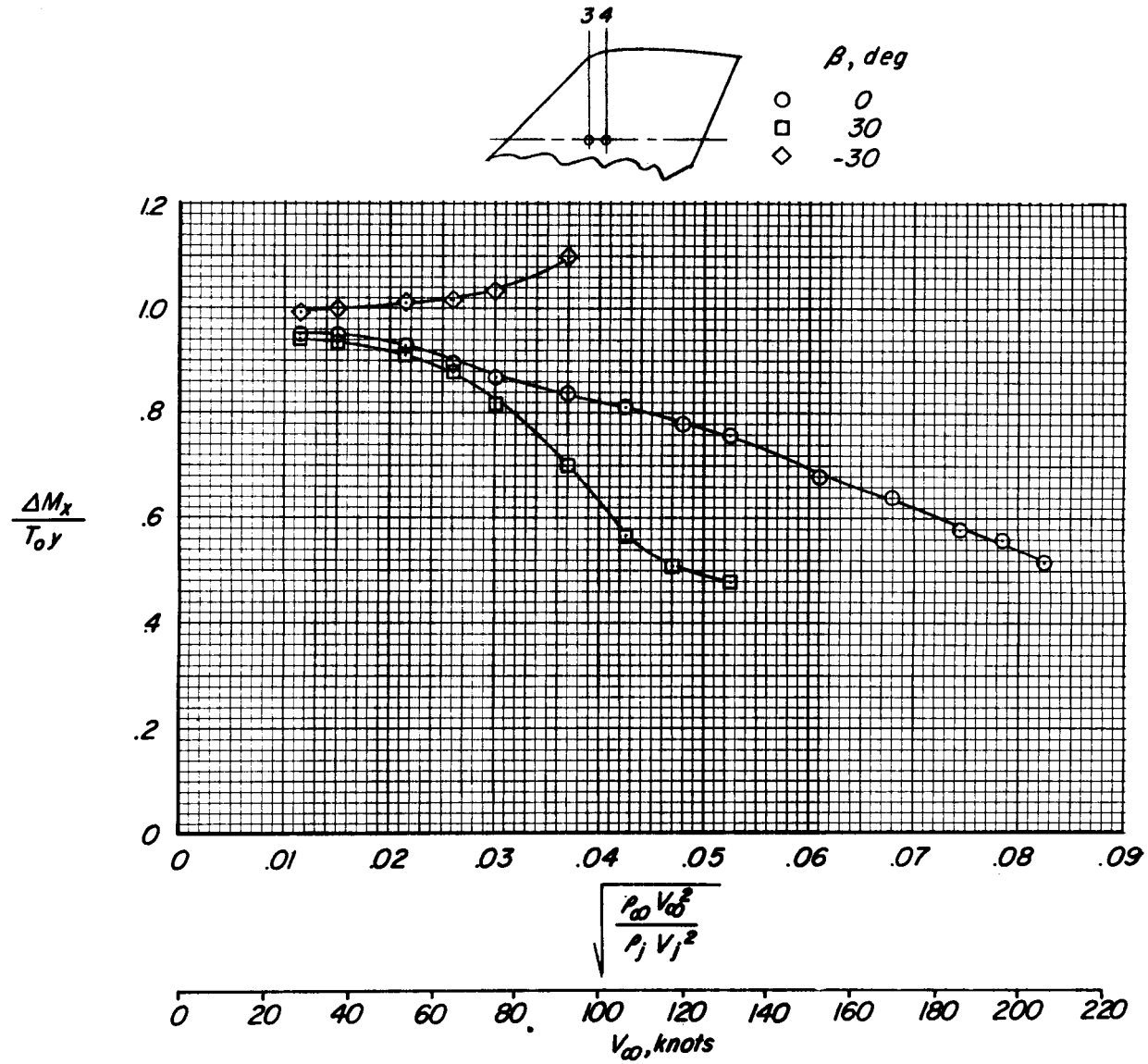

(b) Jet positions 3 and 4.

Figure 10.- Continued.

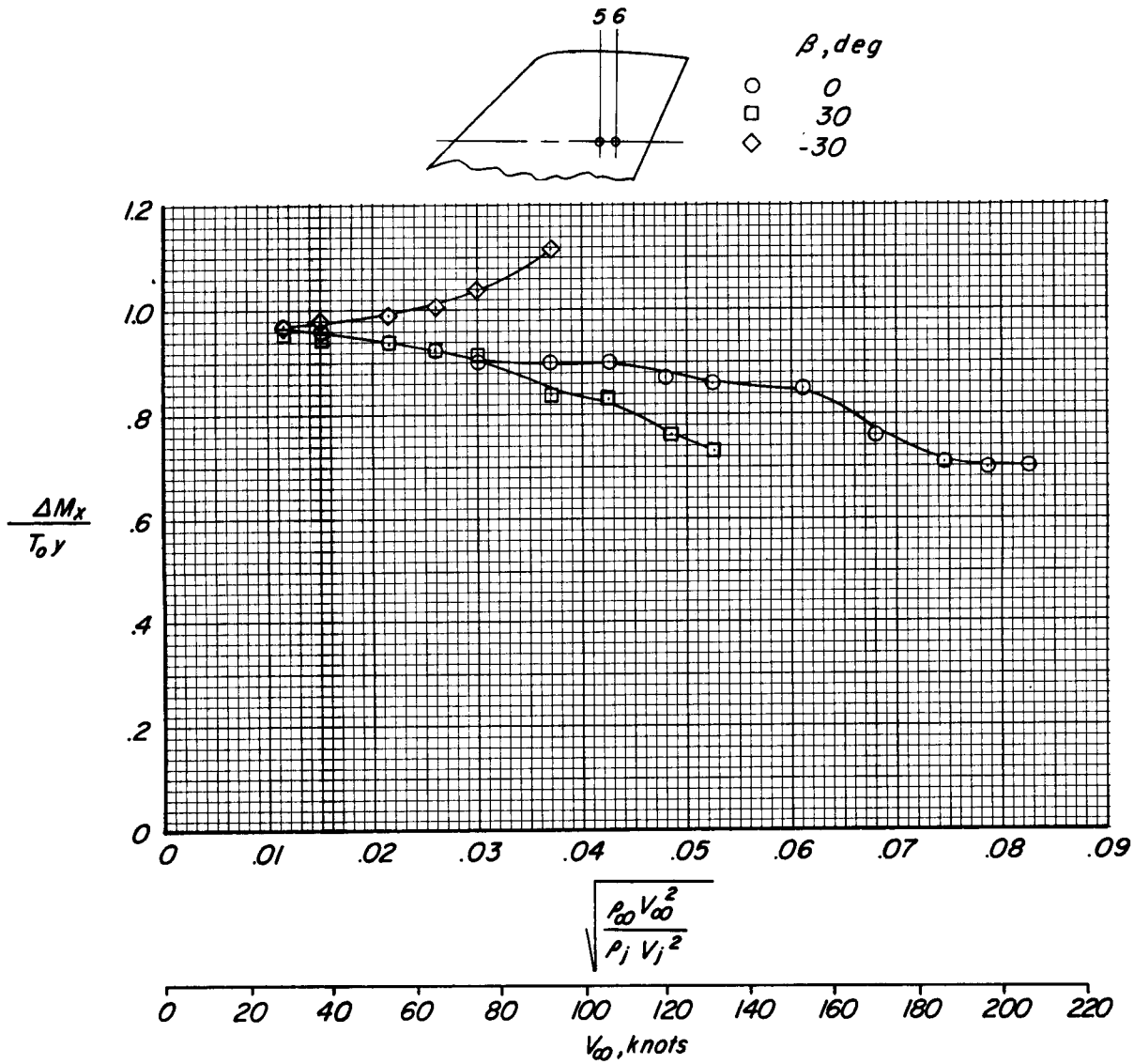

(c) Jet positions 5 and 6.

Figure 10.- Concluded.

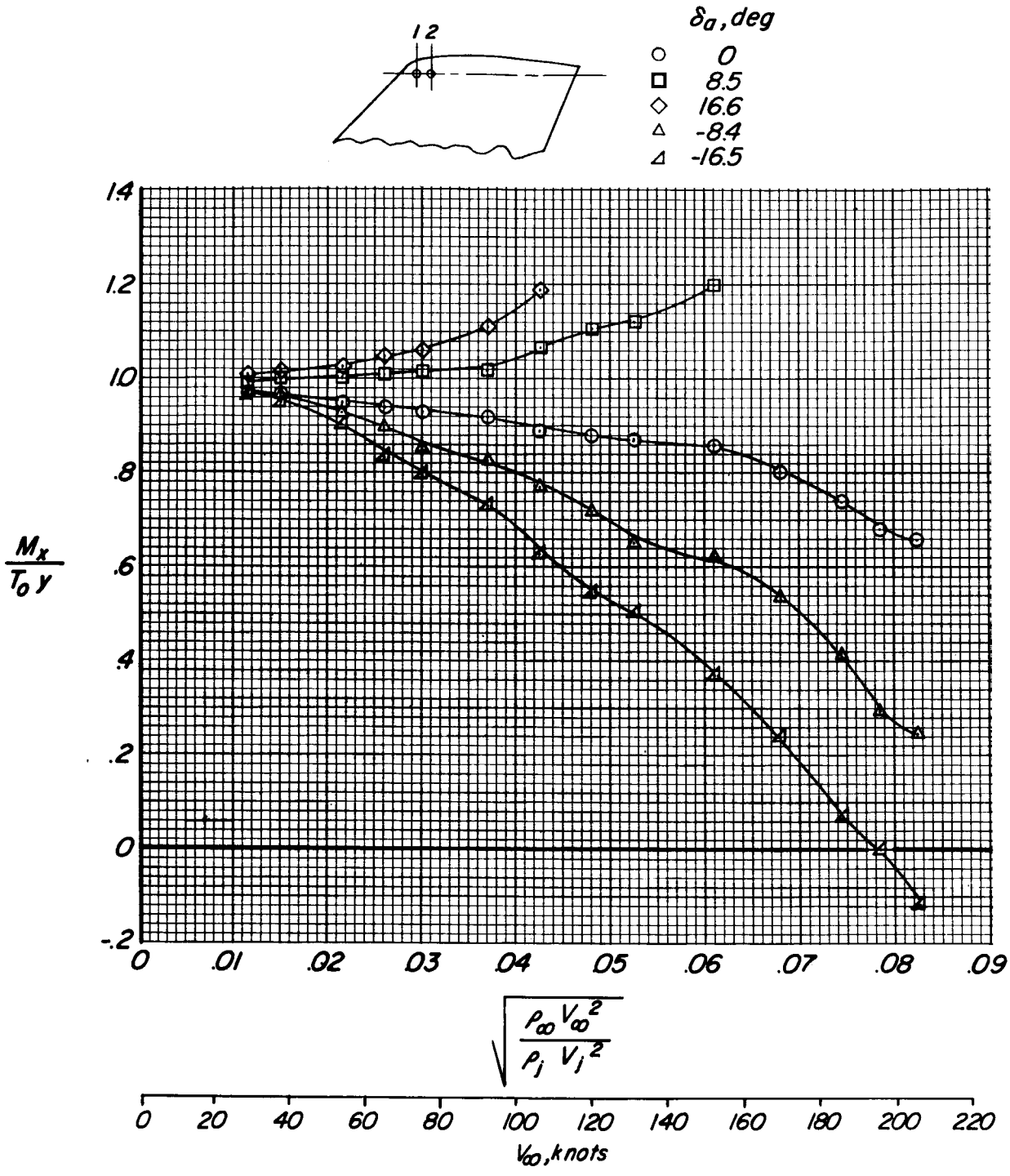

(a) Jet postions 1 and 2.

Figure 11.- Rolling moment due to combined jet, aileron deflection and interference through the transition speed range. Jets at wing tip; $\beta = 0^0$; $p_j/p_\infty = 6.0$.

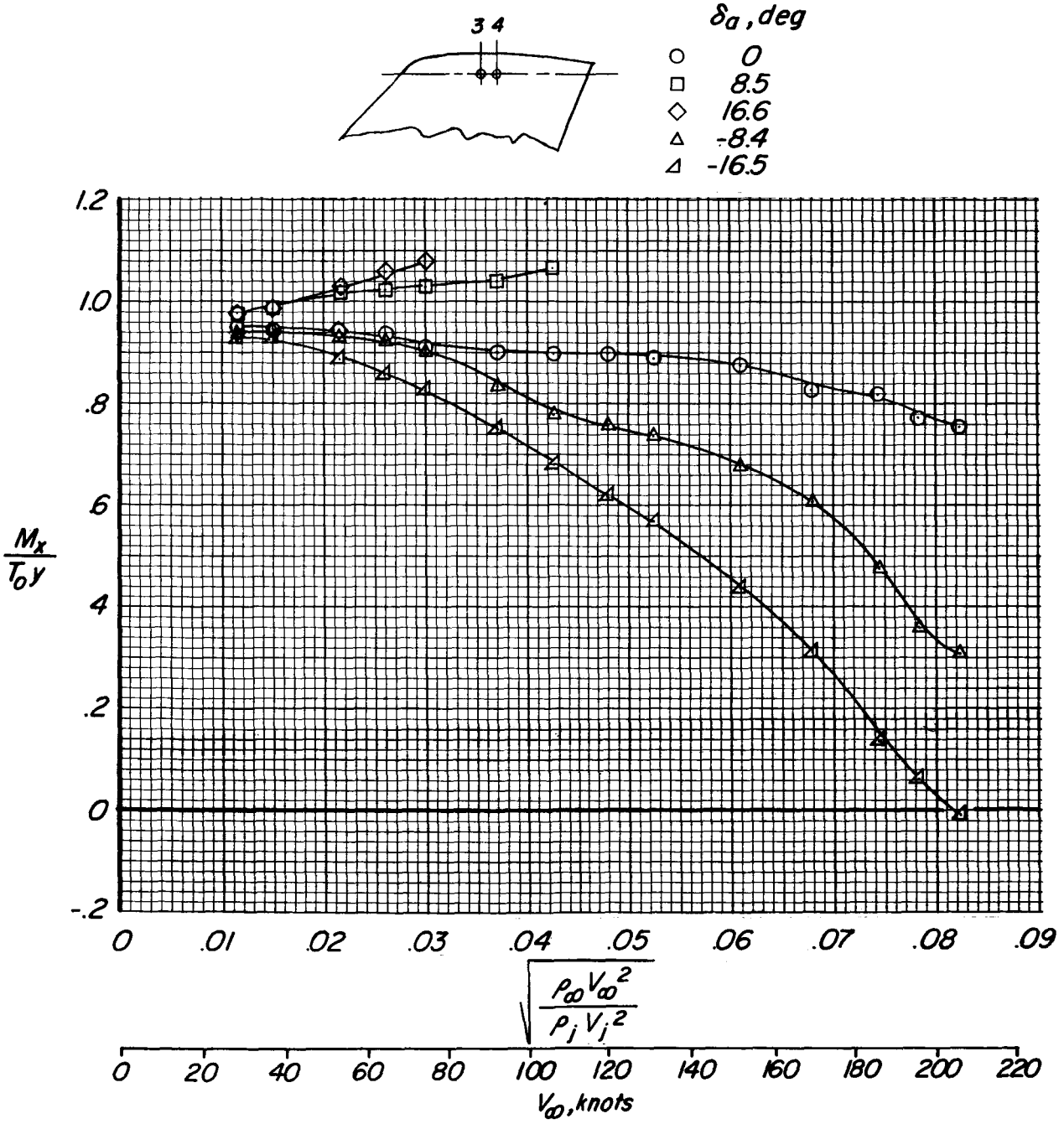

(b) Jet positions 3 and 4.

Figure 11.- Continued.

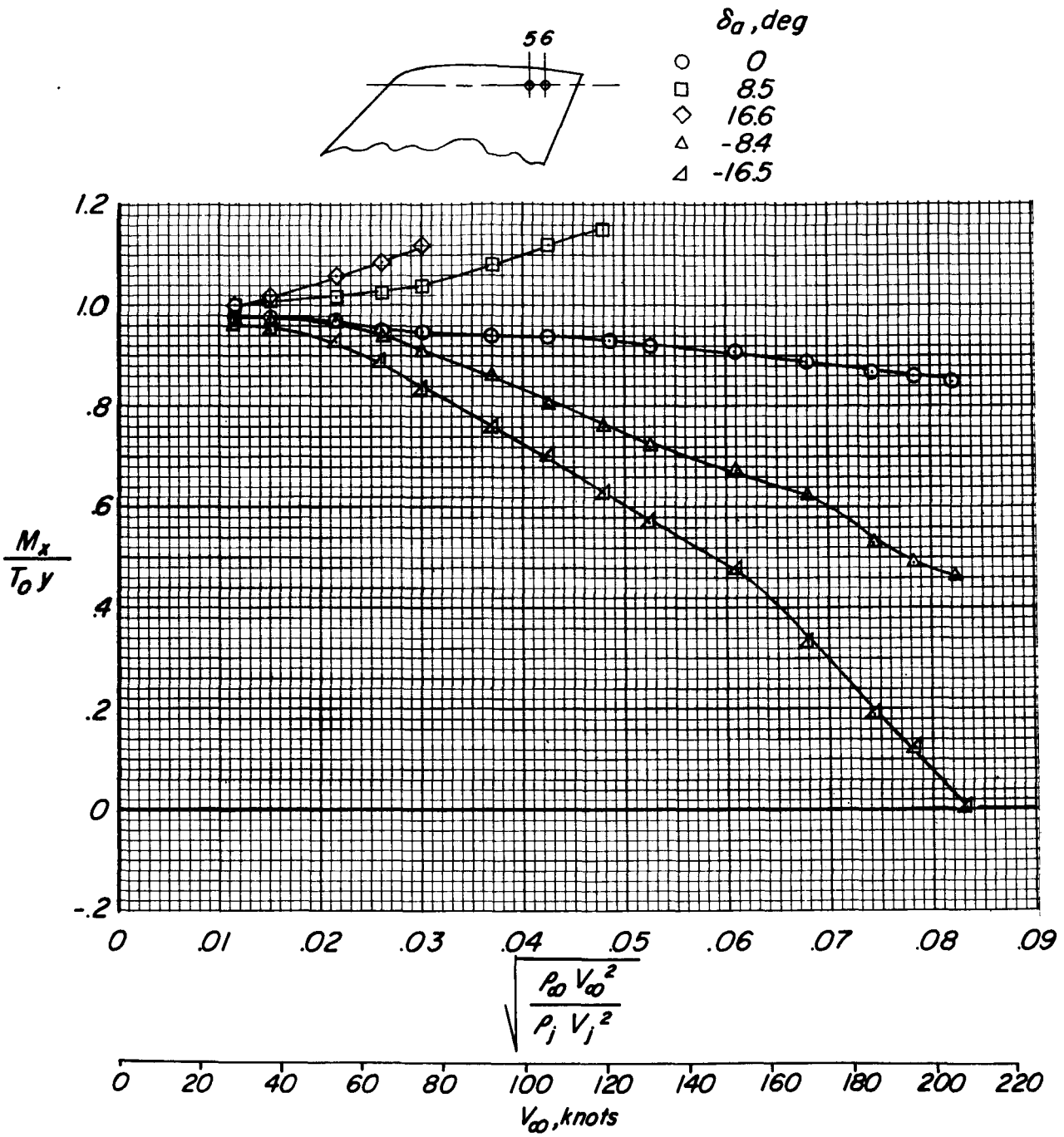

(c) Jet positions 5 and 6.

Figure 11.- Concluded.

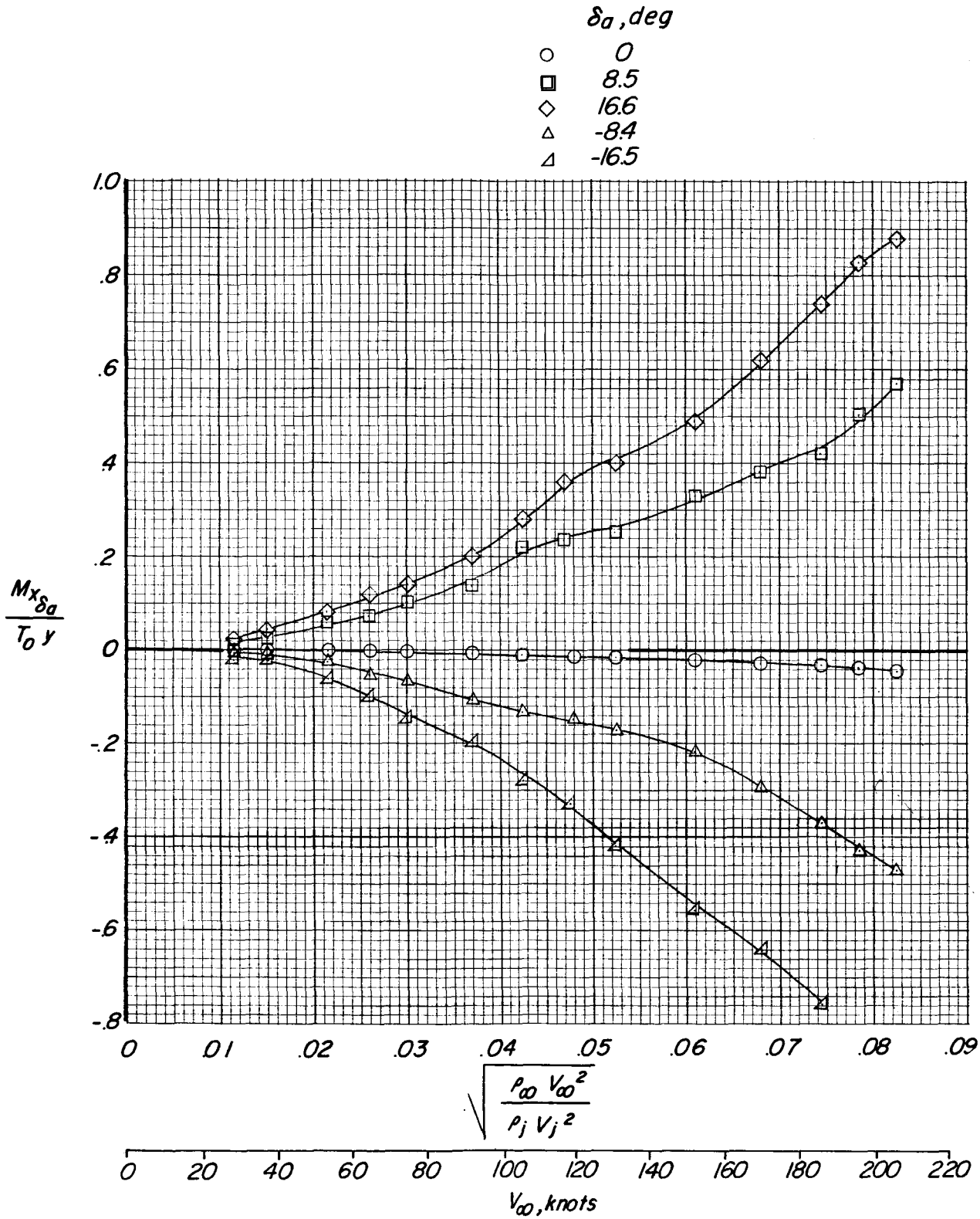

Figure 12.- Rolling moment due to aileron deflection (jets off) nondimensionalized based on power-on condition. Short-span wing; $\beta = 0^0$.

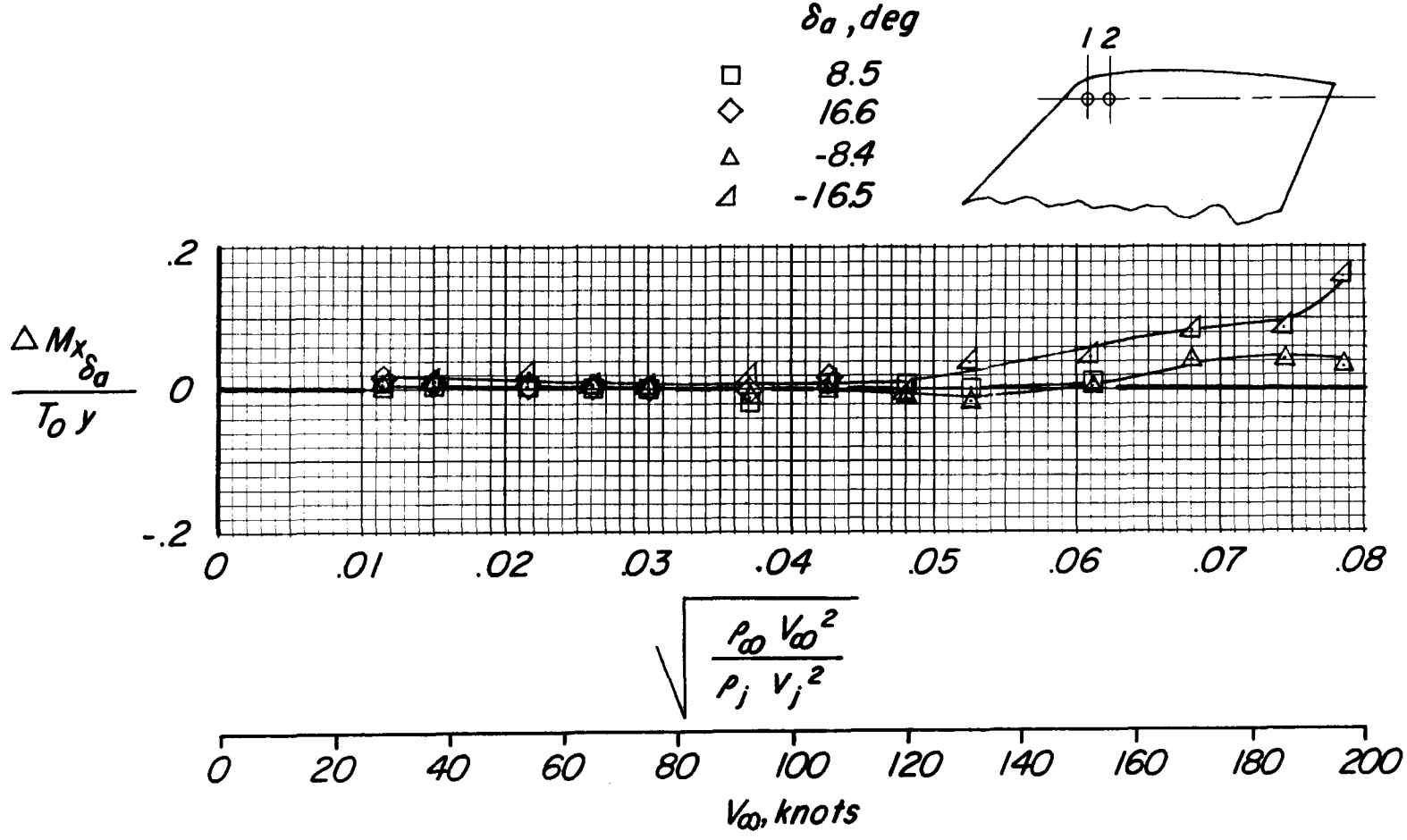

(a) Jet positions 1 and 2.

Figure 13.- Interference increment in rolling moment due to aileron deflection. Jets at wing tip; $\beta = 0^0$; $p_j/p_\infty = 6.0$.

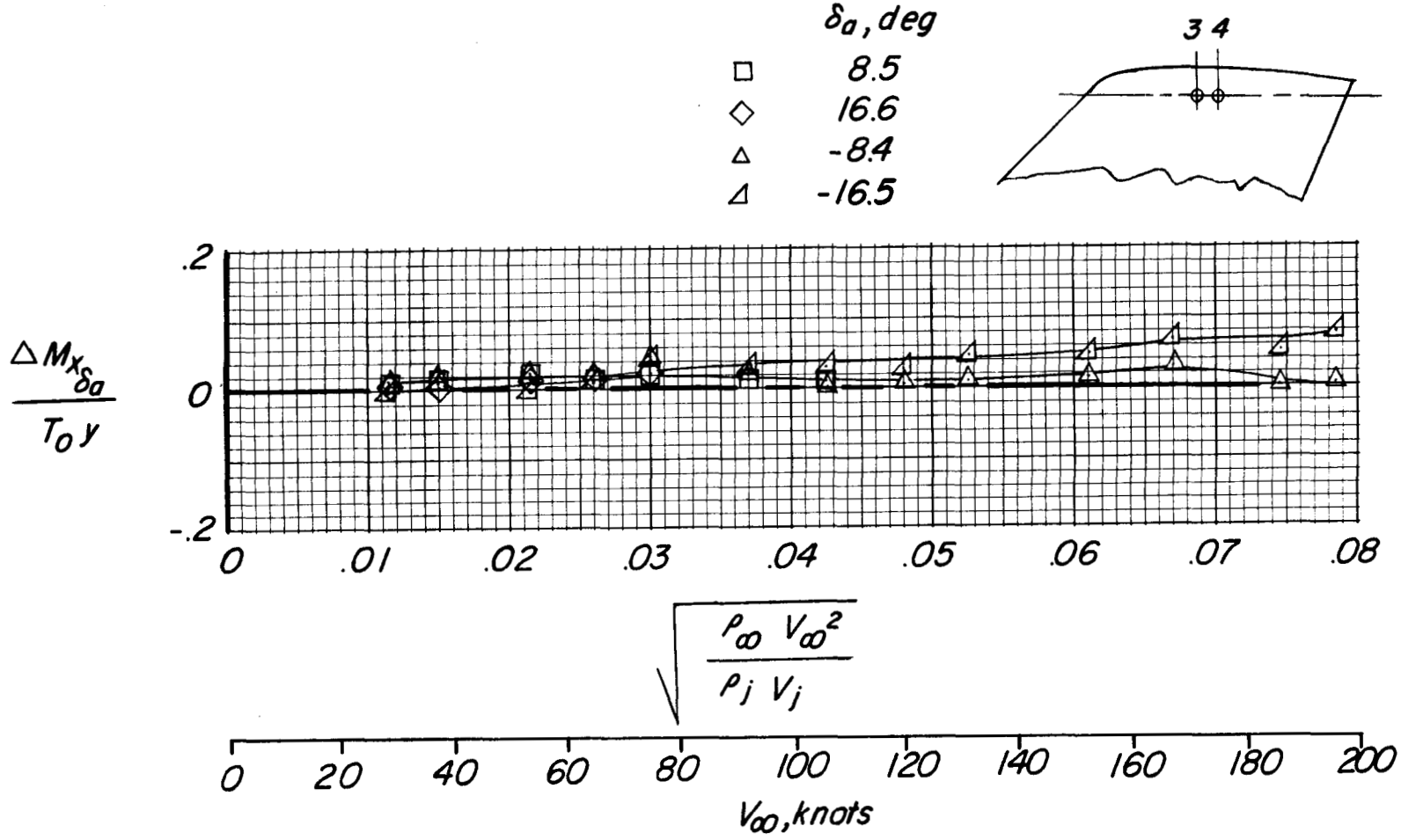

(b) Jet positions 3 and 4.

Figure 13.- Continued.

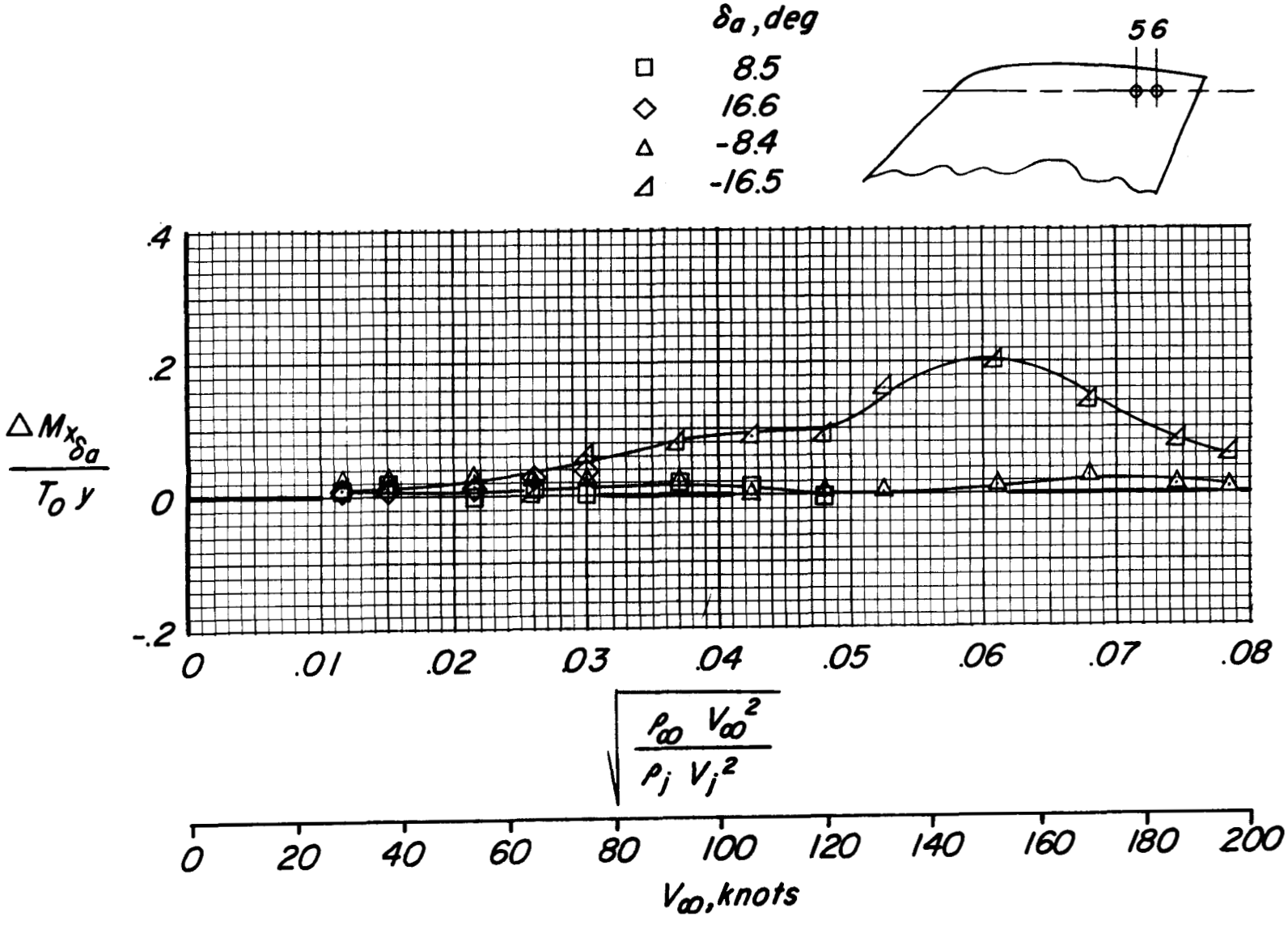

(c) Jet positions 5 and 6.

Figure 13.- Concluded.

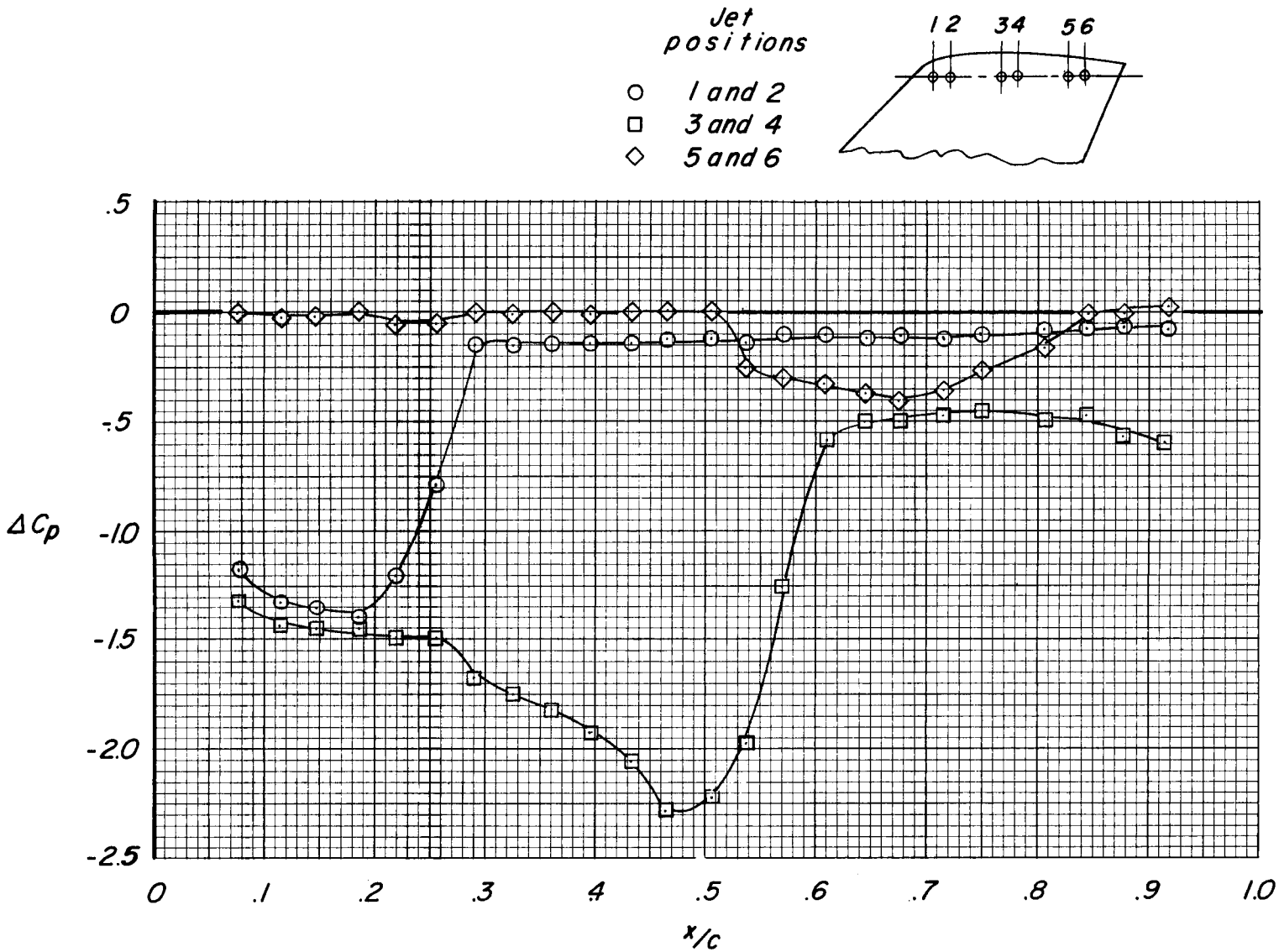

(a) $\beta = 0^0$.

Figure 14.- Typical pressure distribution on wing lower surface near emitting jets. Jets at wing tip; $\delta_a = 0^0$; $\sqrt{\frac{\rho_\infty V_\infty^2}{p_j V_j^2}} = 0.0230 \approx 38.4$ knots; $p_j/p_\infty = 3.6$.

See figure 6.

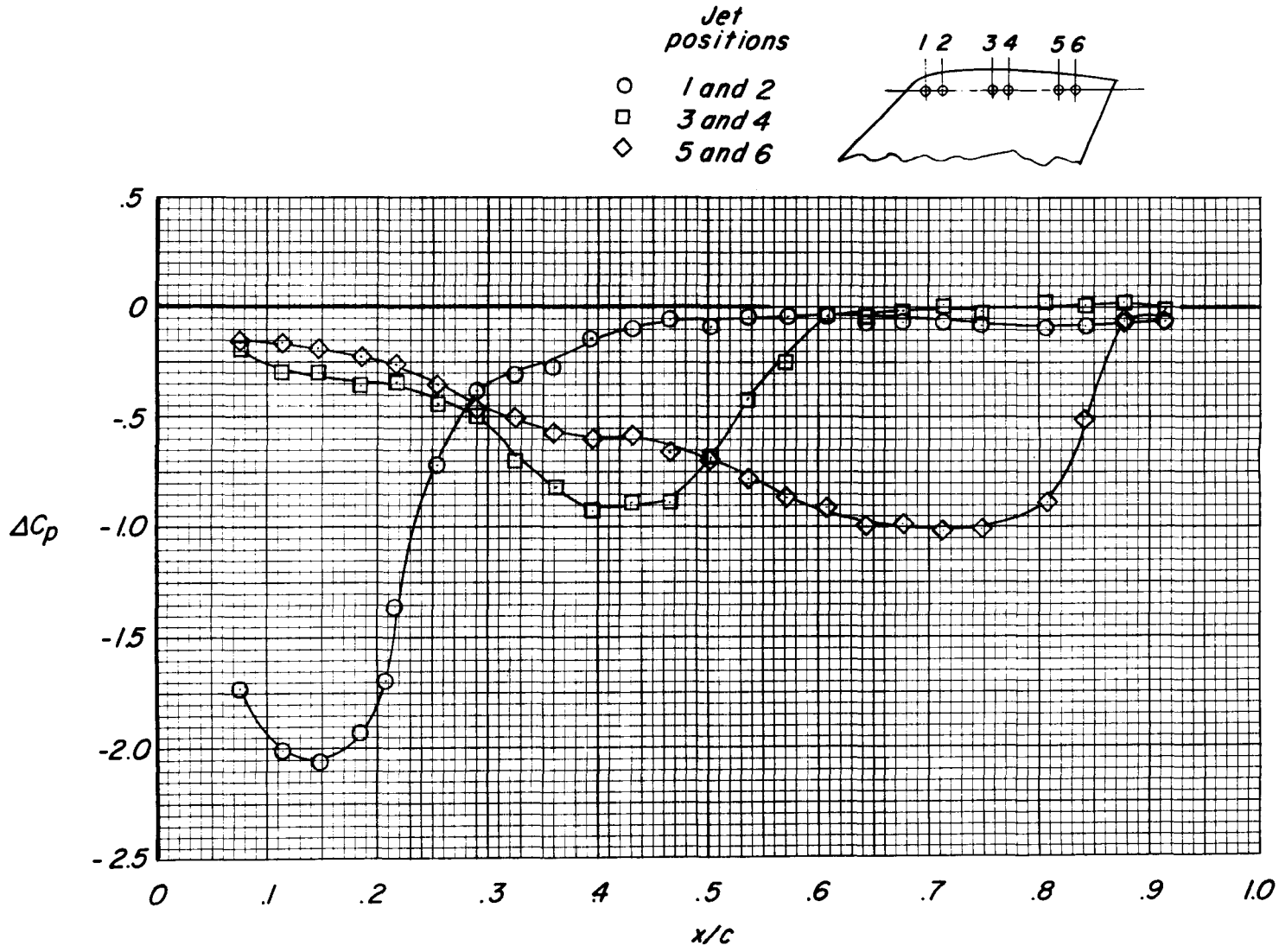

(b) $\beta = 30^{0}$.

Figure 14.- Continued.

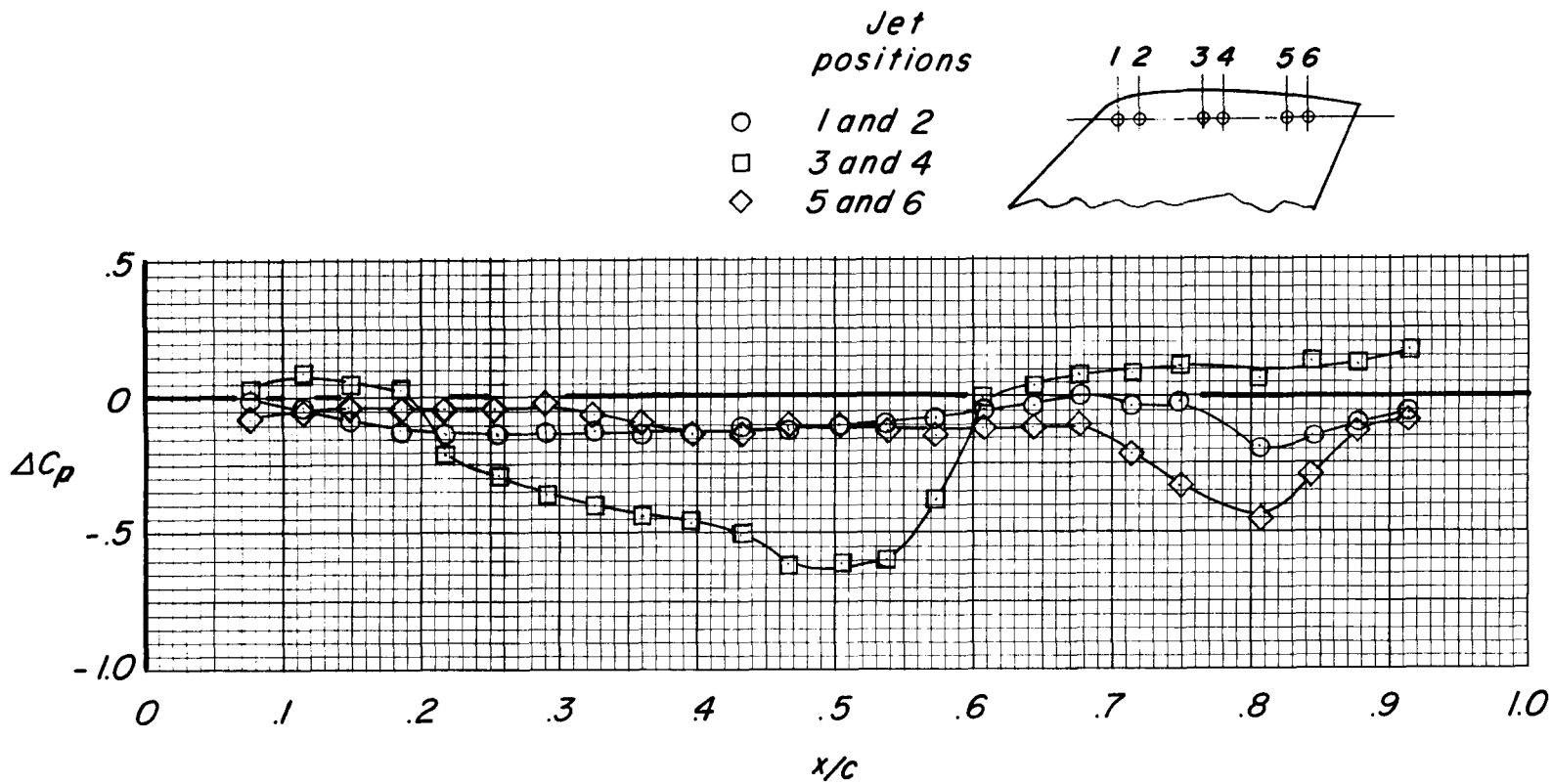

(c) $\beta = -30^{0}$.

Figure 14.- Concluded.

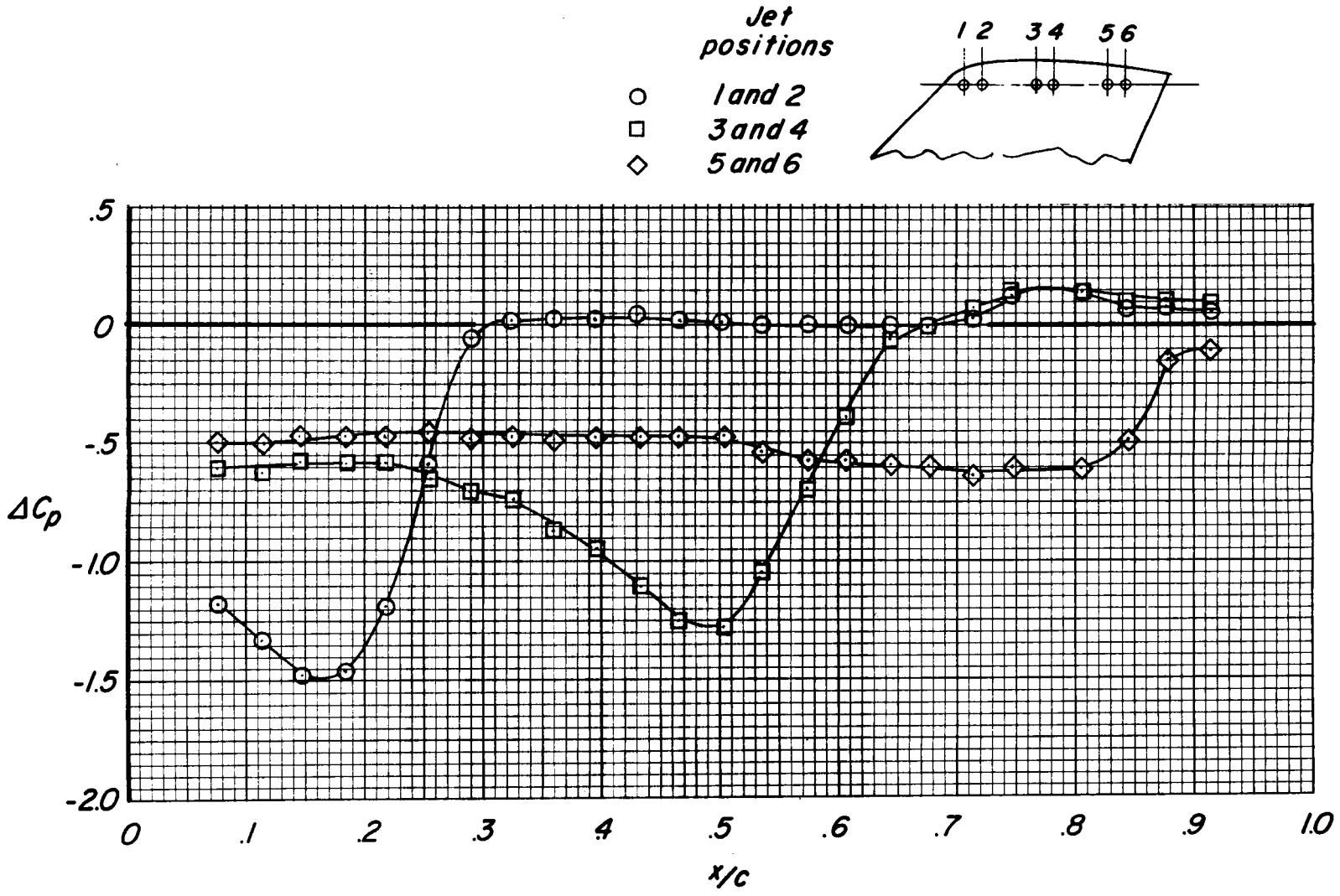

(a) $\beta = 0^{0}$.

Figure 15.- Typical pressure distribution on wing lower surface near emitting jets. Jets at wing tip; $\delta_a = 0^{0}$; $\sqrt{\frac{\rho_\infty V_\infty^2}{\rho_j V_j^2}} = 0.0152 \approx 38.4$ knots; $p_j/p_o = 6.0$. See figure 7.

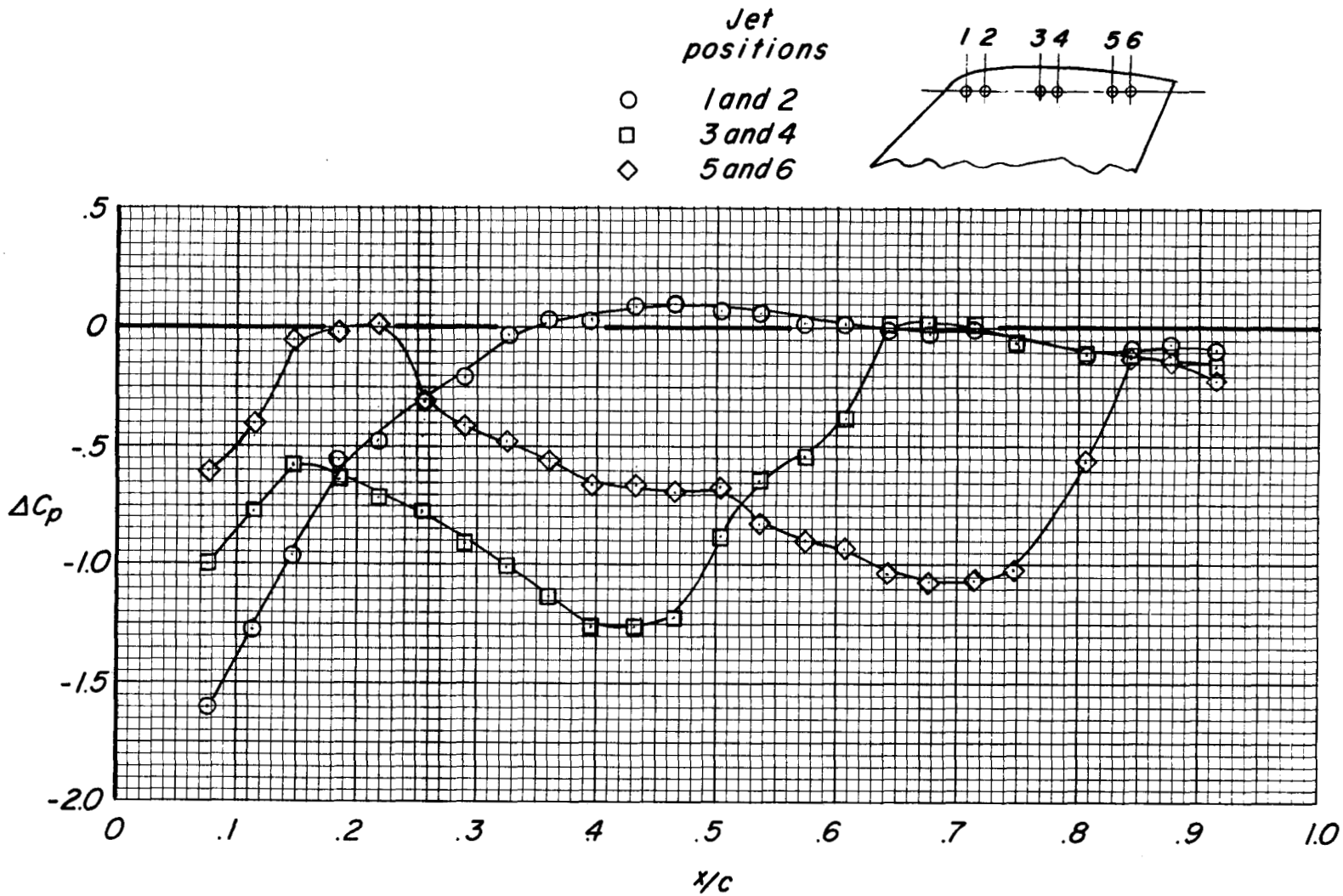

(b) $\beta = 30^0$.

Figure 15.- Continued.

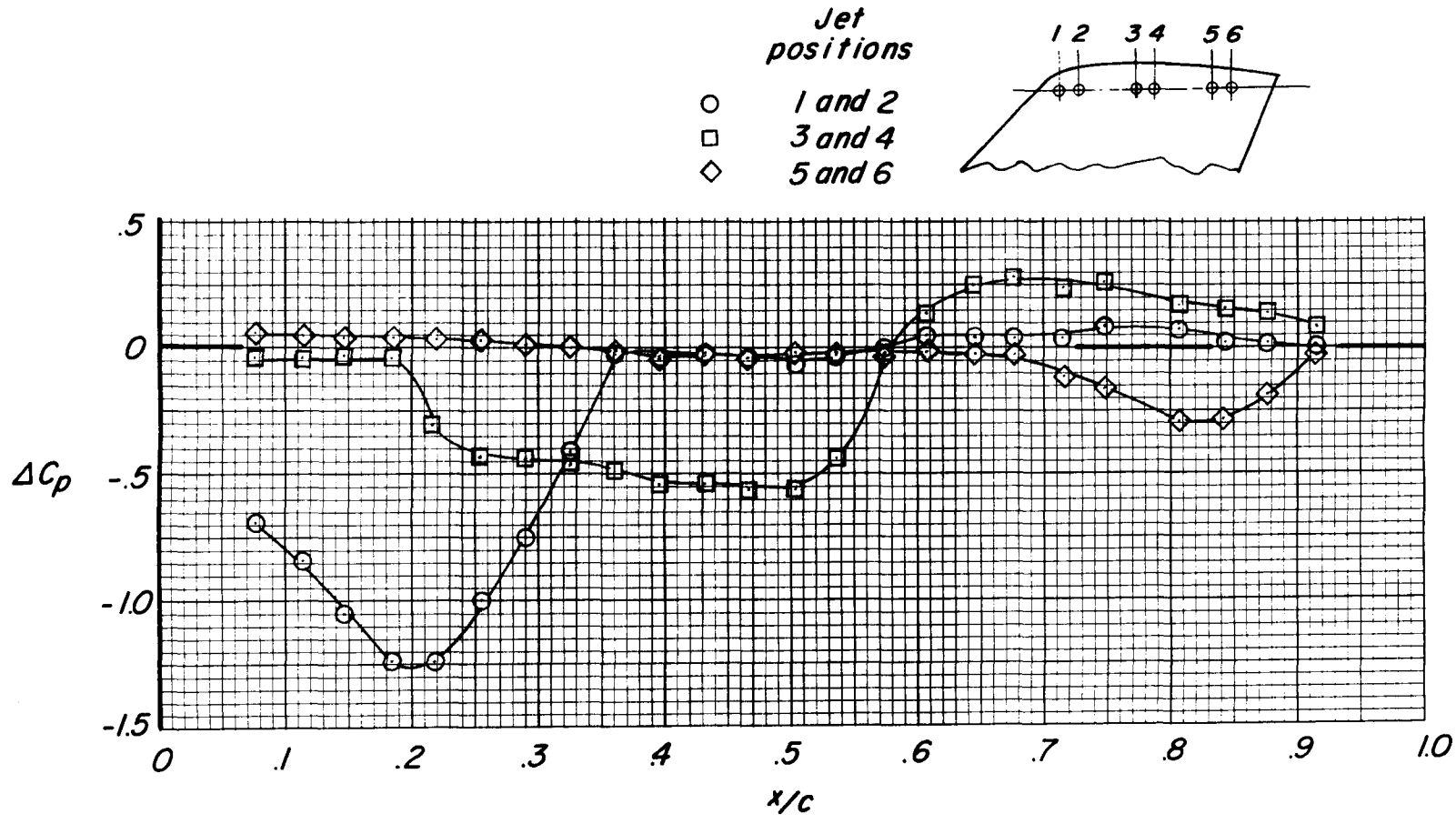

(c) $\beta = -30^{0}$.

Figure 15.- Concluded.

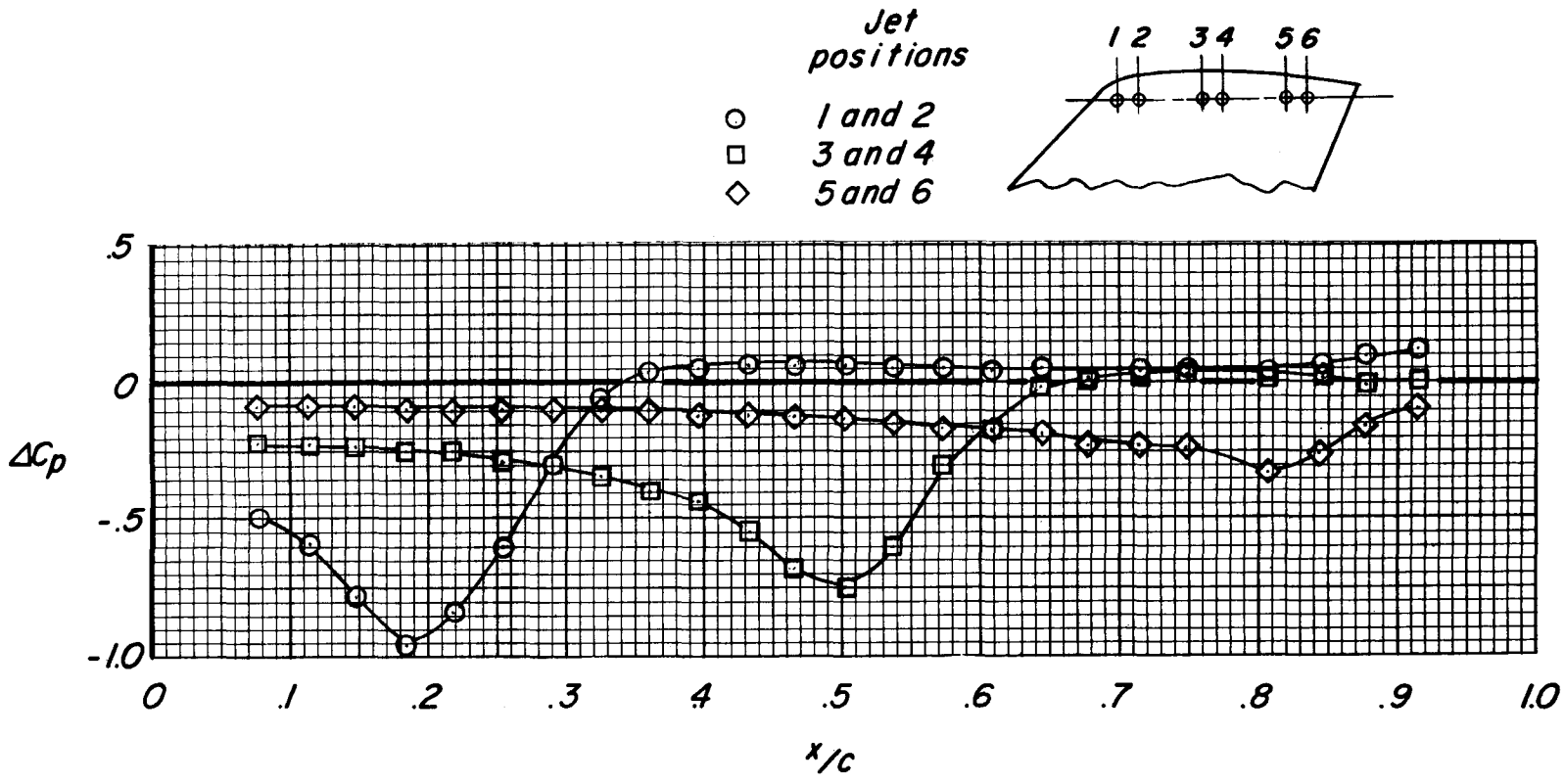

(a) $\beta = 0^0$.

Figure 16.- Typical pressure distribution on wing lower surface near emitting jets. Jets at wing tip; $\delta_a = 0^0$; $\sqrt{\frac{\rho_\infty V_\infty^2}{\rho_j V_j^2}} = 0.0300 \approx 76.7$ knots; $p_j/p_0 = 6.0$.
See figure 7.

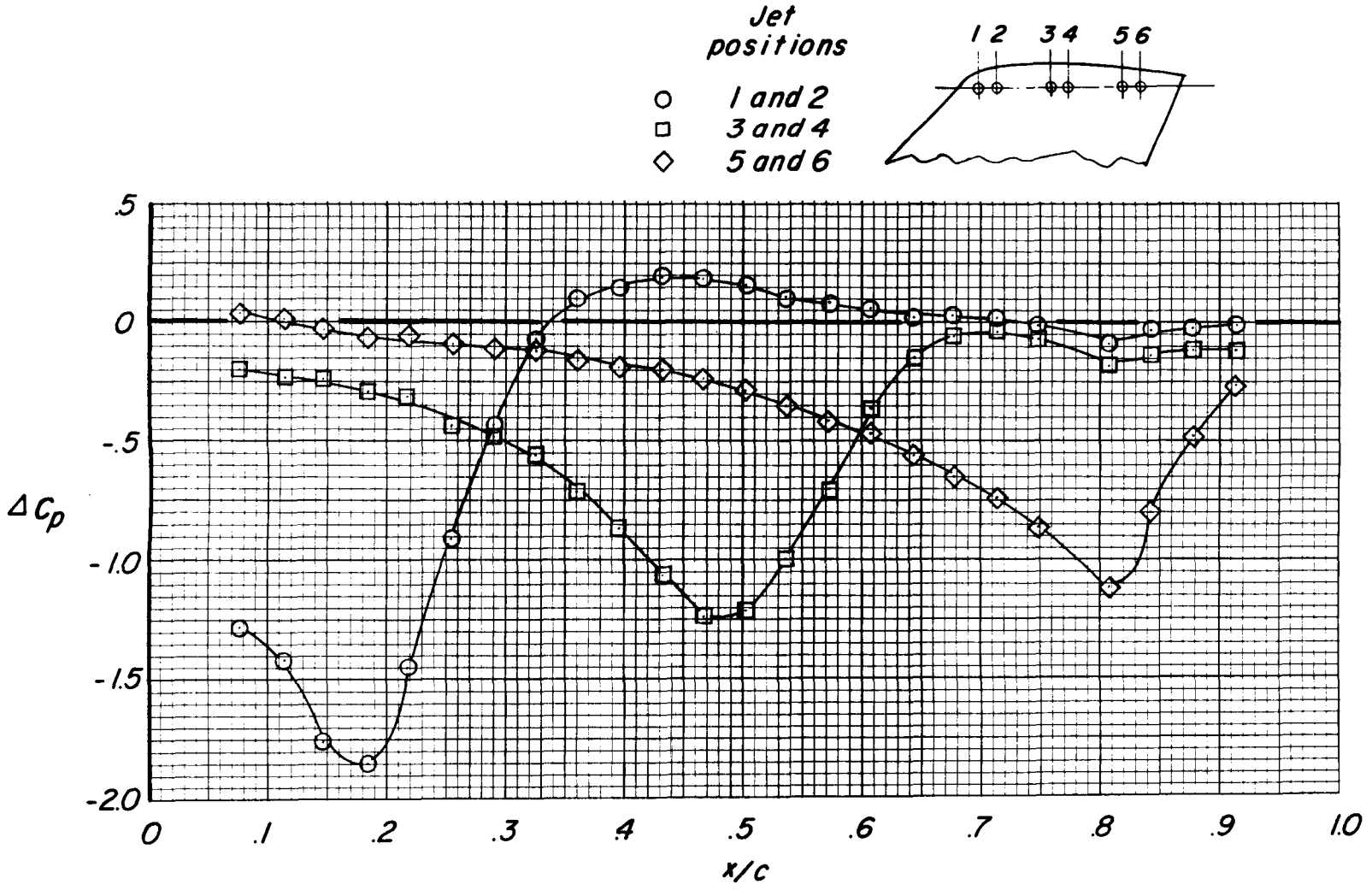

(b) $\beta = 30^0$.

Figure 16.- Continued.

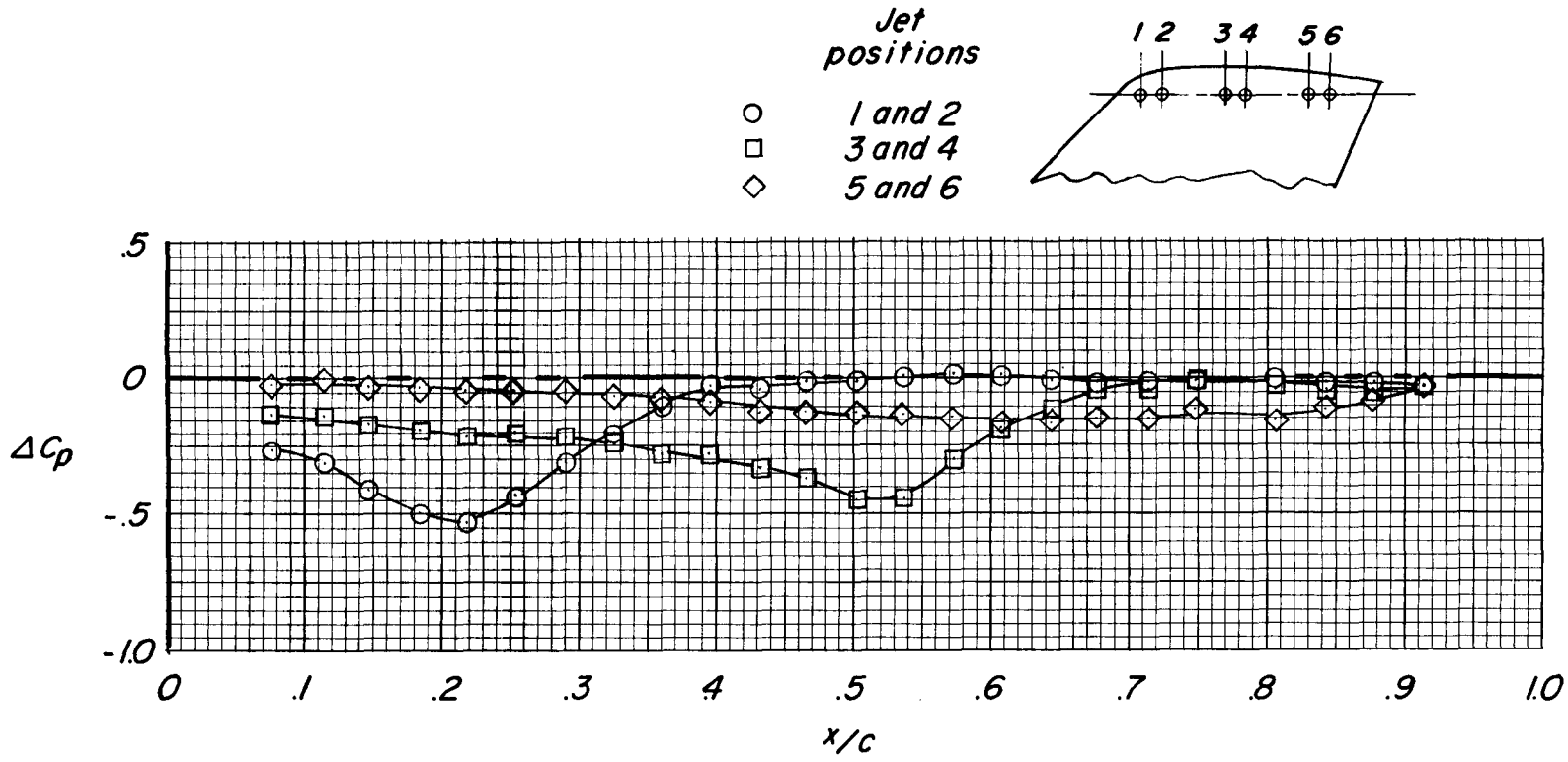

(c) $\beta = -30^0$.

Figure 16.- Concluded.

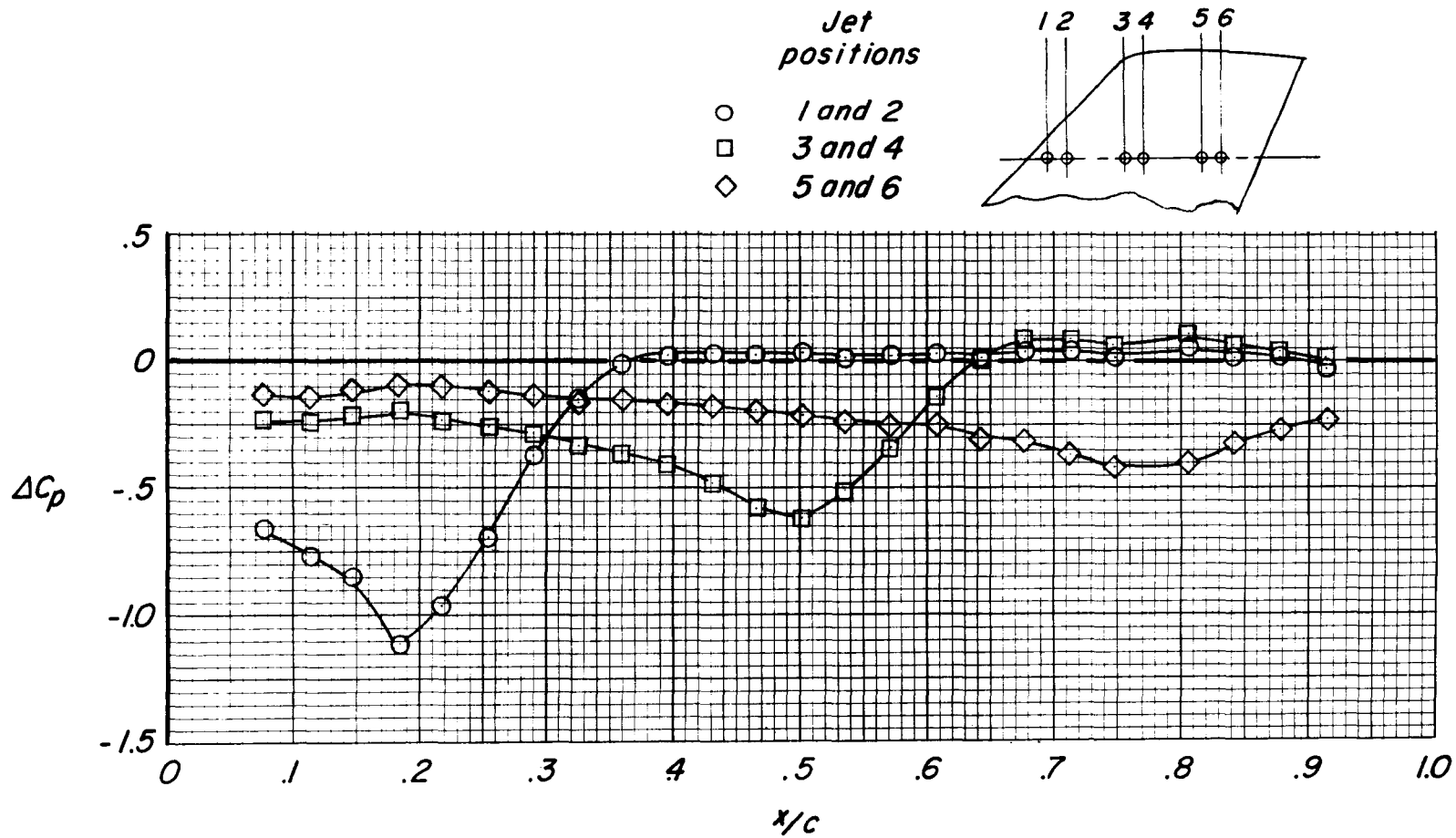

(a) $\beta = 0^0$.

Figure 17.- Typical pressure distribution on wing lower surface near emitting jets. Jets inboard of wing tip; $\delta_a = 0^0$; $\sqrt{\frac{\rho_\infty V_\infty^2}{\rho_j V_j^2}} = 0.0300 \approx 76.7$ knots; $p_j/p_0 = 6.0$.
See figure 8.

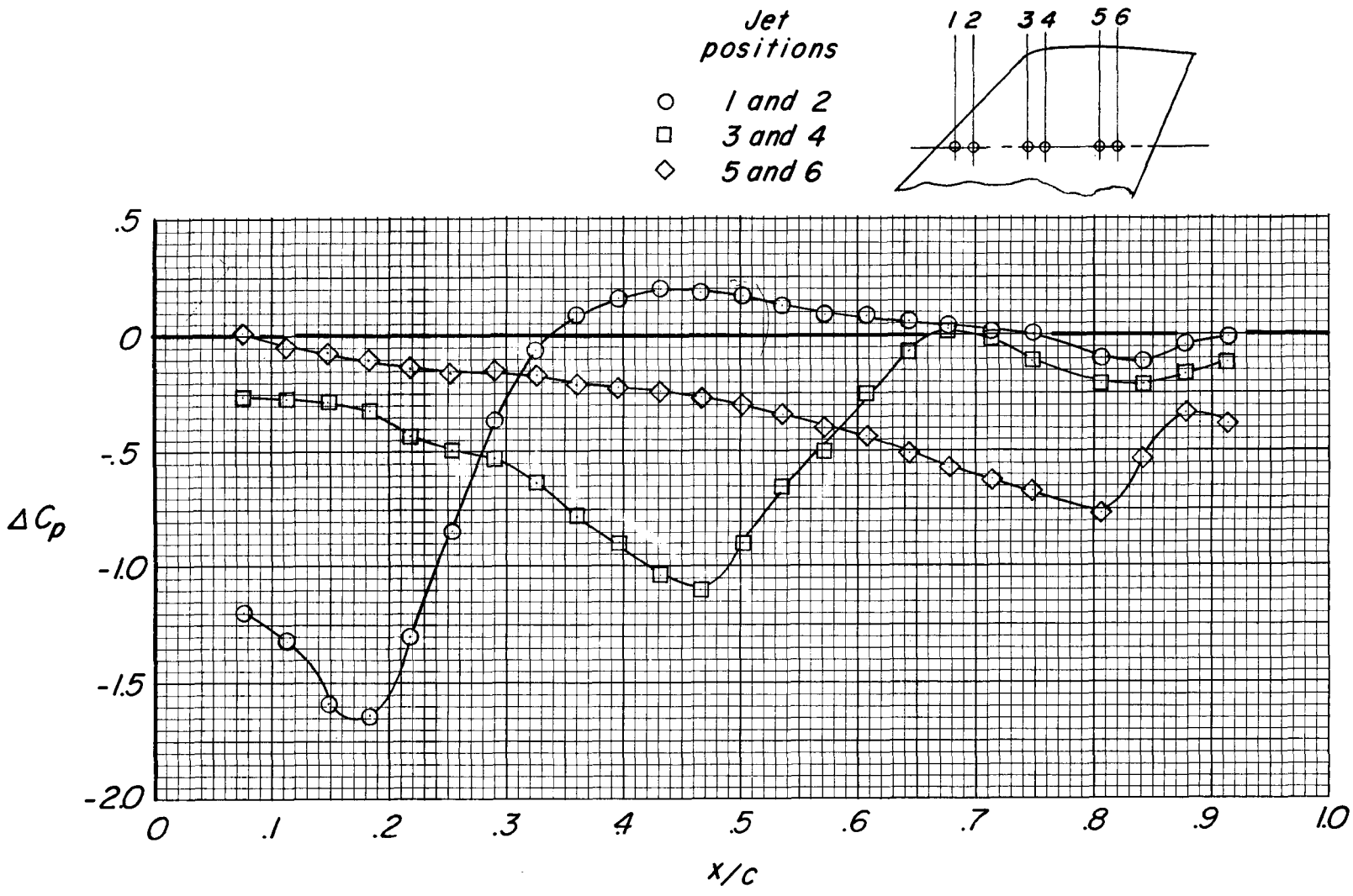

(b) $\beta = 30^0$.

Figure 17.- Continued.

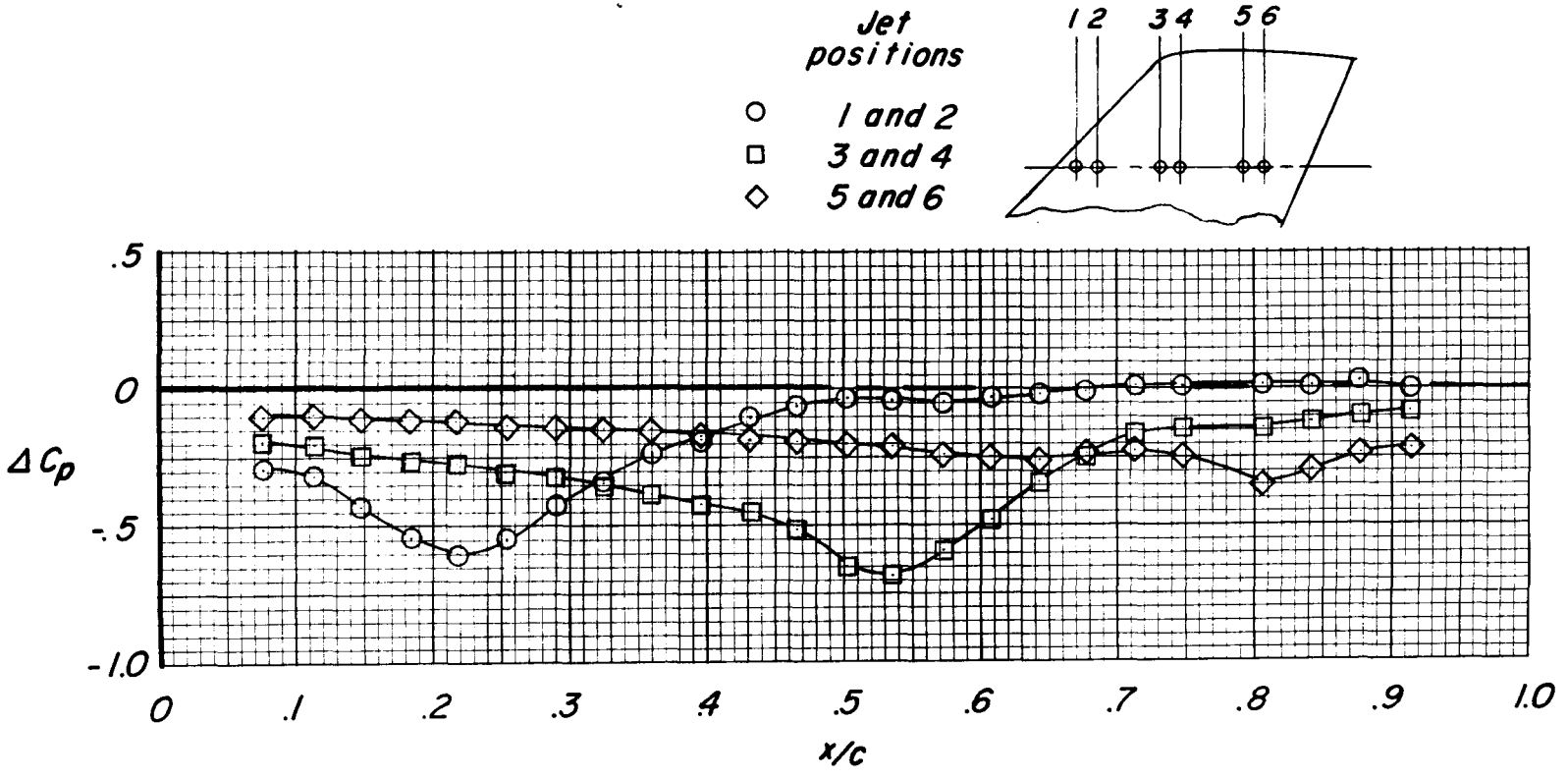

(c) $\beta = -30^{0}$.

Figure 17.- Concluded.

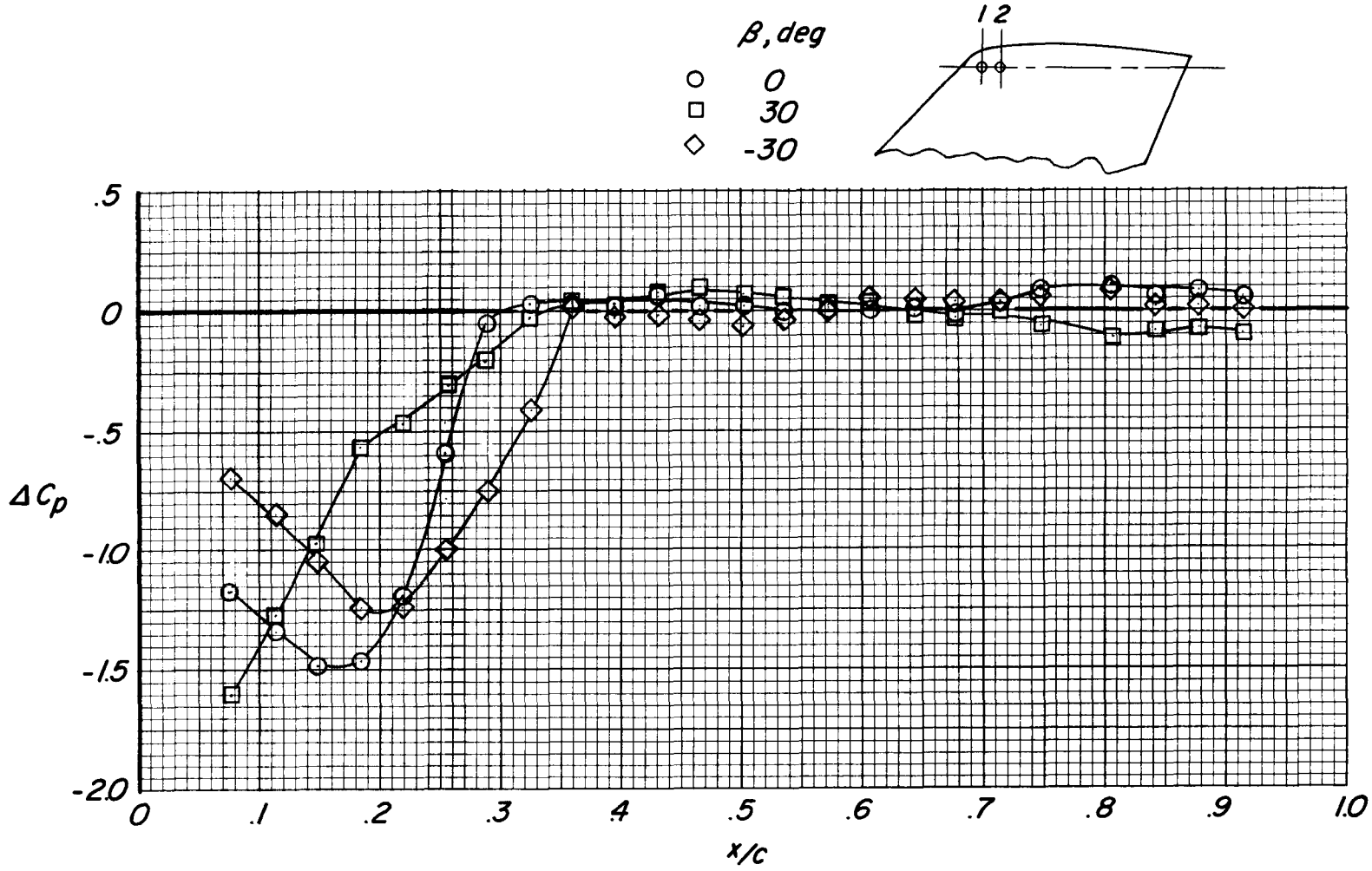

(a) Jet positions 1 and 2.

Figure 18.- Typical pressure distribution on wing lower surface near emitting jets. Jets at wing tip; $\delta_a = 0^0$; $\sqrt{\frac{\rho_\infty V_\infty^2}{\rho_j V_j^2}} = 0.0152 \approx 38.4$ knots; $p_j/p_\infty = 6.0$. See figure 10.

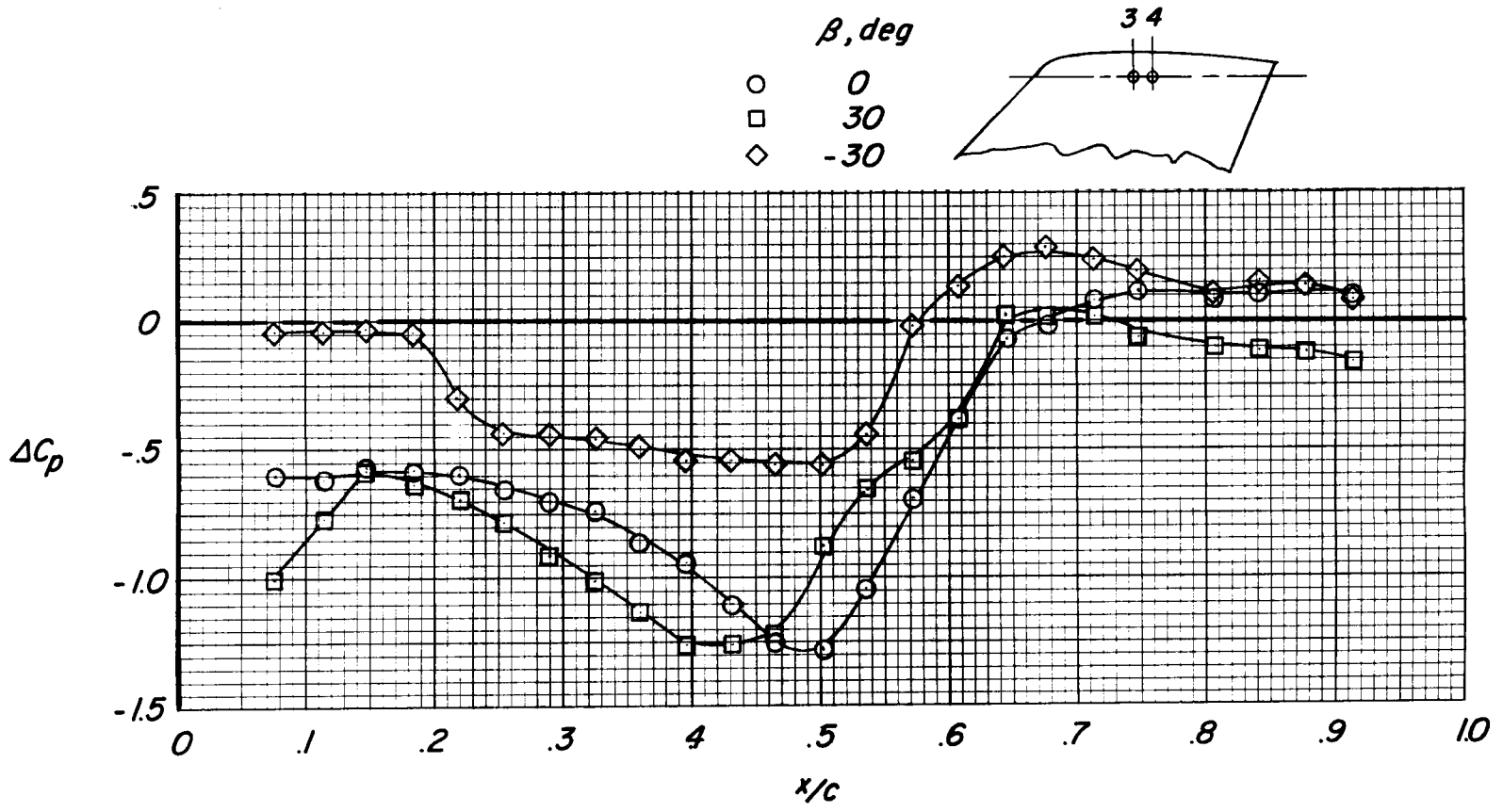

(b) Jet positions 3 and 4.

Figure 18.- Continued.

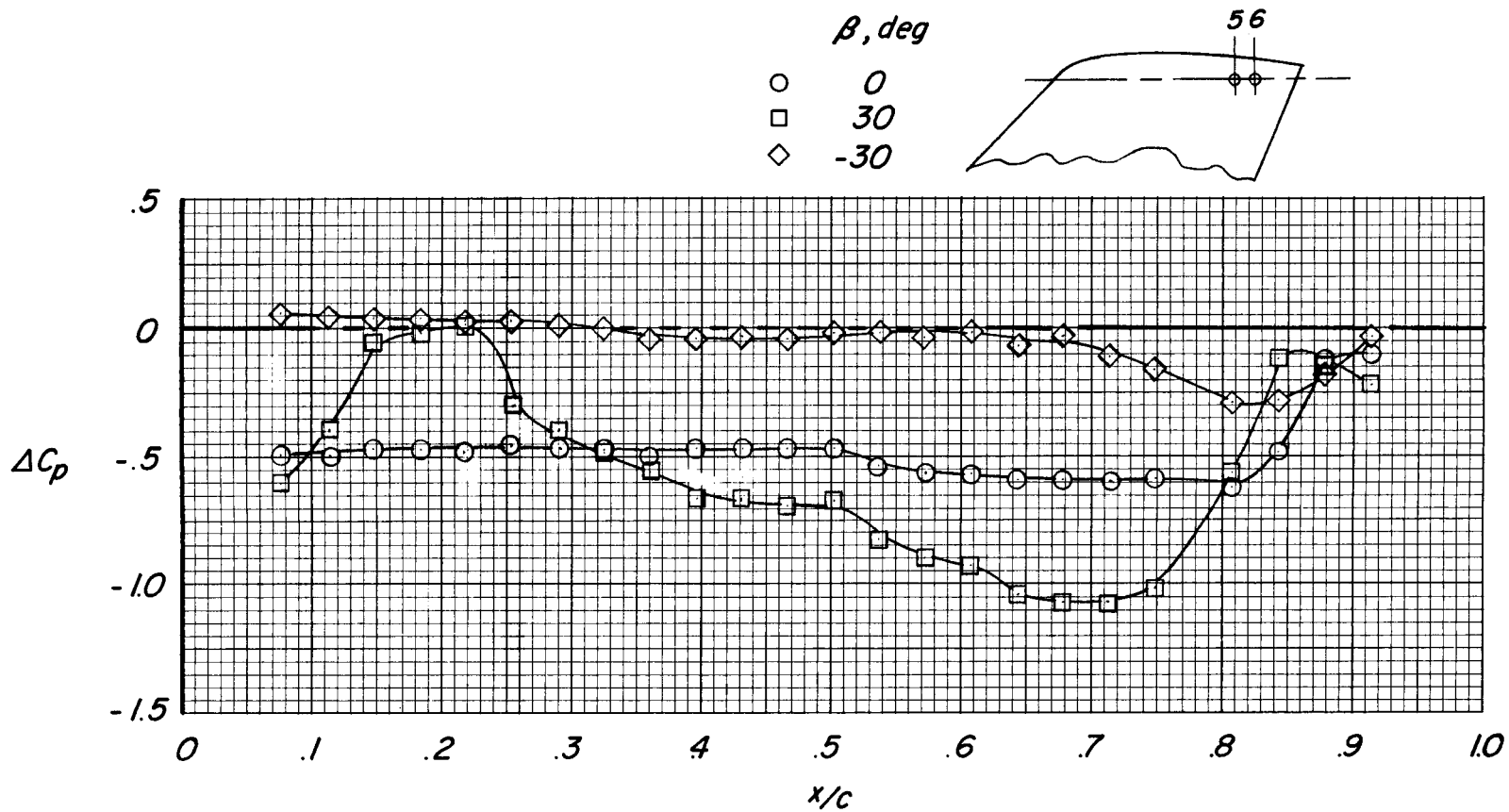

(c) Jet positions 5 and 6.

Figure 18.- Concluded.

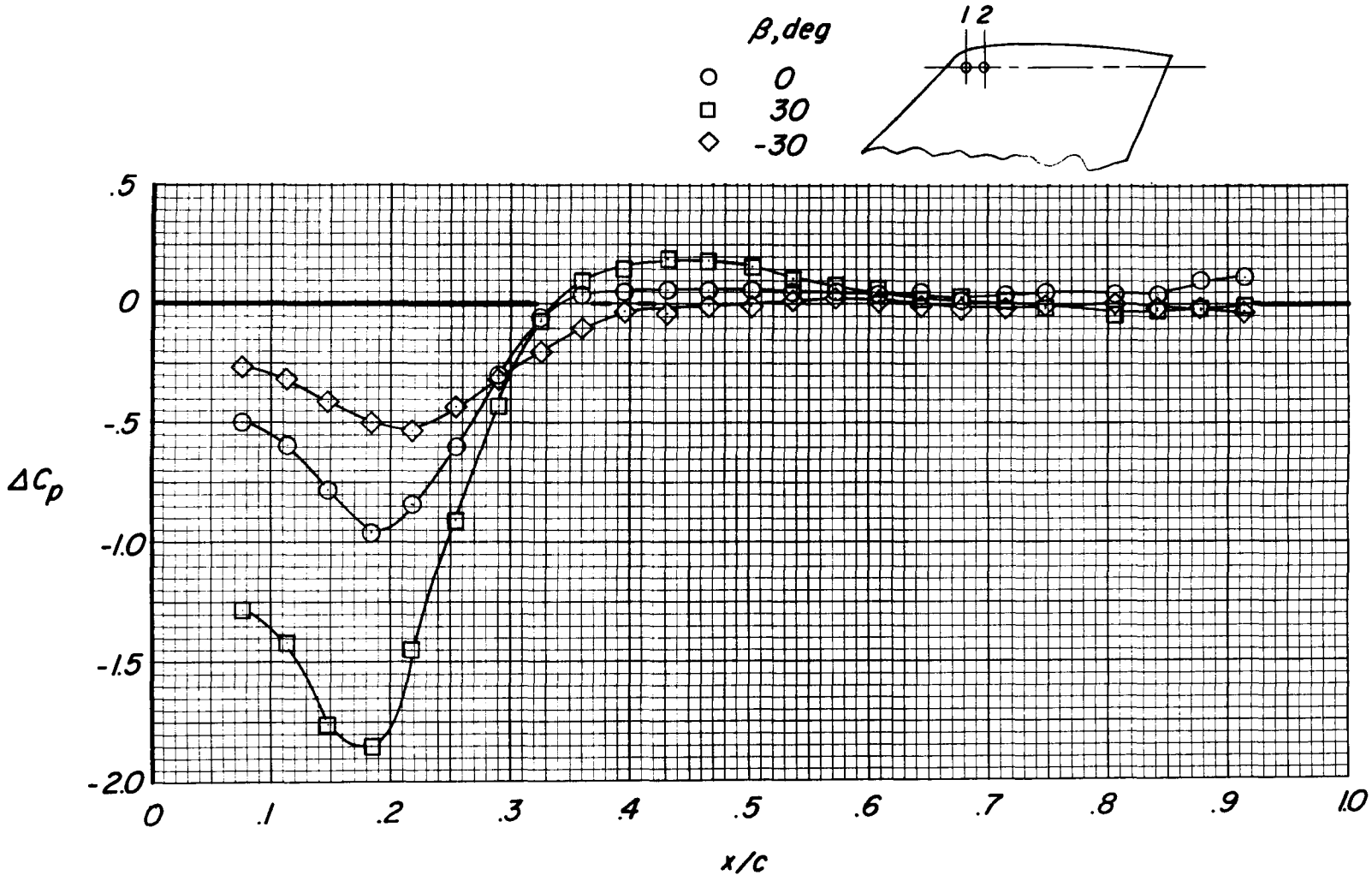

(a) Jet positions 1 and 2.

Figure 19.- Typical pressure distribution on wing lower surface near emitting jets. Jets at wing tip; $\delta_a = 0^o$; $\sqrt{\frac{\rho_\infty V_\infty^2}{\rho_j V_j^2}} = 0.0300 \approx 76.7$ knots; $p_j/p_\infty = 6.0$. See figure 10.

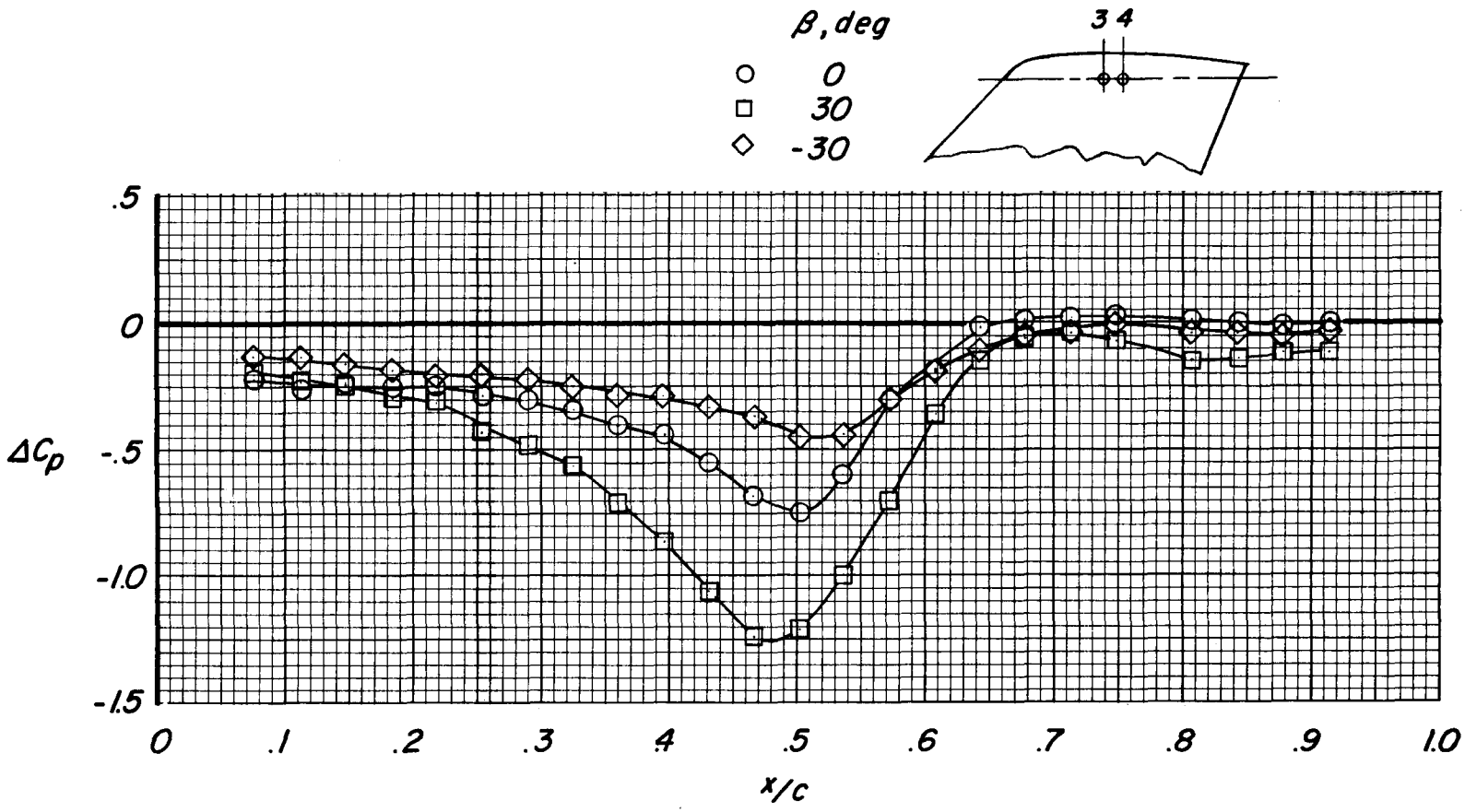

(b) Jet positions 3 and 4.

Figure 19.- Continued.

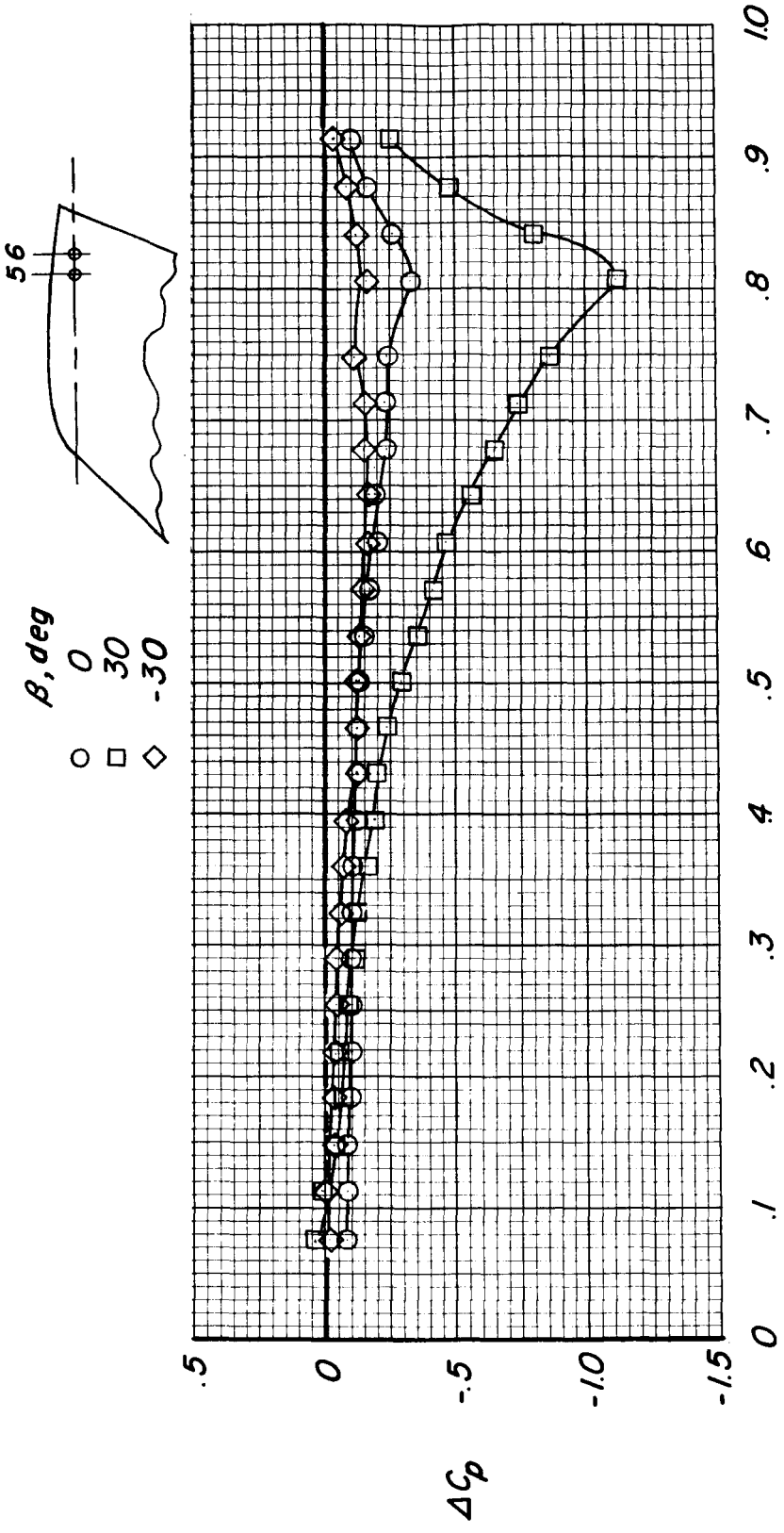

(c) Jet positions 5 and 6.

Figure 19.- Concluded.

NASA-Langley, 1967 — 2 L-5320

"The aeronautical and space activities of the United States shall be conducted so as to contribute . . . to the expansion of human knowledge of phenomena in the atmosphere and space. The Administration shall provide for the widest practicable and appropriate dissemination of information concerning its activities and the results thereof."

—NATIONAL AERONAUTICS AND SPACE ACT OF 1958

NASA SCIENTIFIC AND TECHNICAL PUBLICATIONS

TECHNICAL REPORTS: Scientific and technical information considered important, complete, and a lasting contribution to existing knowledge.

TECHNICAL NOTES: Information less broad in scope but nevertheless of importance as a contribution to existing knowledge.

TECHNICAL MEMORANDUMS: Information receiving limited distribution because of preliminary data, security classification, or other reasons.

CONTRACTOR REPORTS: Scientific and technical information generated under a NASA contract or grant and considered an important contribution to existing knowledge.

TECHNICAL TRANSLATIONS: Information published in a foreign language considered to merit NASA distribution in English.

SPECIAL PUBLICATIONS: Information derived from or of value to NASA activities. Publications include conference proceedings, monographs, data compilations, handbooks, sourcebooks, and special bibliographies.

TECHNOLOGY UTILIZATION PUBLICATIONS: Information on technology used by NASA that may be of particular interest in commercial and other non-aerospace applications. Publications include Tech Briefs, Technology Utilization Reports and Notes, and Technology Surveys.

Details on the availability of these publications may be obtained from:

SCIENTIFIC AND TECHNICAL INFORMATION DIVISION

NATIONAL AERONAUTICS AND SPACE ADMINISTRATION

Washington, D.C. 20546